Journal of Cleaner Production 407 (2023) 137056

Contents lists available at ScienceDirect

Journal of Cleaner Production

journal homepage: www.elsevier.com/locate/jclepro

A framework for assessing uncertainty of drinking water quality in distribution networks with application to monochloramine decay

Matthew Frankel [a], Lynn E. Katz [a], Kerry Kinney [a], Charles J. Werth [a], Corwin Zigler [b], Lina Sela [a,*]

[a] Department of Civil, Architectural and Environmental Engineering, The University of Texas at Austin, 301 East Dean Keeton St, Austin, 78712, TX, United States of America

[b] Department of Statistics and Data Science, The University of Texas at Austin, 105 East 24th St, Austin, 78705, TX, United States of America

ARTICLE INFO

Handling Editor: Jing Meng

Keywords:
Uncertainty analysis
Monochloramine decay
Water supply systems
EPANET MSX

ABSTRACT

To analyze changes in water quality conditions in water distribution systems (WDS), such as disinfectant byproduct formation, chlorine residual, and biofilm growth, water utilities can use coupled hydraulic and chemical models. Model-based operational decisions are complicated by uncertainties in model input parameters, which propagate through the model resulting in uncertain model predictions. Previous works have focused on conducting sensitivity analyses of input parameters in various water quality reactions and the interactions with hydraulic factors, but have overlooked the specific contribution of hydraulic and chemical parameter uncertainty. In this work, a framework for assessing the hydraulic and chemical uncertainty in water quality models is presented and demonstrated using monochloramine decay in WDSs supplied by gravity and pumping systems. In the first step, a sensitivity analysis is conducted to determine the influential and non-influential chemical parameters which govern the rate of monochloramine decay. In the second step, Monte Carlo simulations are used to explore the individual and combined effects of uncertainty in hydraulic and chemical parameters. Results show that uncertainty in modeled monochloramine concentration increases with water age and higher reaction rates, varies throughout the course of a day, and heavily depends on hydraulic variability, emphasizing the need to account for input uncertainty. The computational tool developed in this work can be extended to other reaction mechanisms, water quality parameters, and distribution systems for case-specific conditions, and used to evaluate system-wide effects of uncertainty on water quality.

1. Introduction

The core function of municipal water utilities is to ensure safe and reliable water supply to its consumers. Within the United States, the Safe Drinking Water Act (SDWA) provides the regulatory framework for sufficient water quality, promulgating legal requirements for a variety of chemical constituents (e.g., chlorine residual, disinfection byproducts, turbidity) (Tiemann, 2017). The SDWA details specific locations and frequency of water quality samples at treatment plants, leading to a high degree of certainty regarding the quality of water as it leaves the treatment plant. However, as water travels from treatment plants to consumers through a complex network of pipes in the water distribution system (WDS), chemical reactions, such as decay of chlorine residual (Pasha and Lansey, 2010; Pfaller et al., 2021), corrosion of heavy metals (Masters et al., 2016; Lytle and Liggett, 2016), and formation of disinfection byproducts (Chowdhury et al., 2009; Pfaller et al., 2021), impact water quality, which as a result can exhibit high degrees of spatial and temporal variability (Blokker et al., 2014). Water utilities maintain different levels of oversight to ensure adequate water quality by relying on periodic water quality grab sampling at different locations in the WDS following various EPA rules (e.g., Lead and Copper Rule, Total Coliform Rule) (American Water Works Association, 2013). However, these sampling protocols provide limited spatial and temporal coverage of the underlying water quality conditions in the WDS. Hence, there is a higher degree of uncertainty regarding the water quality conditions within a WDS compared to that leaving a treatment plant. To overcome some of these limitations, coupled hydraulic and chemical models can be useful tools to quantify changes and predict where diminished water quality may occur (Rossman et al., 2020; Shang et al., 2008; Chang et al., 2012)

Although models can augment grab samples to estimate water quality at all locations within a WDS, due to the deterministic nature of simulation models, even a well-parameterized model excludes the inherent hydraulic and chemical uncertainty within an actual WDS. Therefore, this research proposes a methodology for quantification of

* Corresponding author.
E-mail address: linasela@utexas.edu (L. Sela).

https://doi.org/10.1016/j.jclepro.2023.137056
Received 29 December 2022; Received in revised form 29 March 2023; Accepted 31 March 2023
Available online 6 April 2023

chemical and hydraulic uncertainty in model predictions. The proposed computational framework can be applied to different chemical reactions and species (e.g., chlorine decay, bacterial growth, and thrialometne formation). We demonstrate the application of the proposed framework towards exploring the uncertainty related to the fate of monochloramine in WDSs. Monochloramine is used as a secondary disinfectant in approximately 25% of drinking water utilities in the United States (Alpert et al., 2017). Utilization of monochloramine as a secondary disinfectant has recently increased to enable compliance with the Stage 1 and Stage 2 Disinfectants and Disinfection Byproducts Rules, since the use of monochloramine lowers the levels of disinfection byproduct formation compared to the use of free chlorine (Khiari, 2019). Hence, identifying the key factors contributing to the uncertainty and quantifying the uncertainty related to the fate of monochloramine is critical for model-based decisions for managing water quality in WDSs.

The main mechanism by which hydraulic uncertainty affects water quality is by changing flow conditions. As a result, water age is affected, altering the time that a chemical reaction can occur before water reaches a consumer. Water age is a useful surrogate indicator for water quality, where lower water ages indicate water quality more similar to treatment plant effluent (U.S. Environmental Protection Agency, 2002). Hydraulic factors which affect water age and contribute to uncertainty include fluctuations in consumer demands, residence times and mixing within storage tanks (Gibson et al., 2020) and junctions (Pankaj et al., 2022). A hydraulic model calibrated to the average daily demand, may mischaracterize water quality, if random fluctuations, seasonal variability in water usage, or long-range conservation trends are not considered (Hatam et al., 2021; Abokifa et al., 2020; Zhuang and Sela, 2020).

Uncertainties also exist in the parameterization of chemical reactions, such as rate constants and equilibrium constants that often determined from laboratory experiments and may not be representative of actual drinking water (Morris and Isaac, 1983). Some chemical parameters, e.g., chlorine wall decay rate, are site specific and cannot be measured or experimentally verified. Moreover, some complex chemical processes, such as formation of certain disinfection byproducts, are not adequately characterized, yielding uncertainty when using simplified chemical representations (Zhang et al., 2022).

Previous works have focused on different aspects of chemical and hydraulic uncertainty contributing to water quality in WDSs (Smith, 2013). For example, the authors in Hart et al. (2019) and Rodriguez et al. (2021) have investigated optimal sampling strategies to reduce uncertainty within a WDS by sampling in areas where models suggest greater uncertainty exists. Monte Carlo (MC) analyses have been conducted to determine the effect of model parameters, such as bulk and wall chlorine decay coefficient, pipe diameter and roughness, consumer demands, tank mixing, and contaminant intrusion (Pasha and Lansey, 2010; Gibson et al., 2020; Hart et al., 2019). The authors in Abhijith et al. (2021) developed a simplified reaction scheme between chlorine decay, bacterial growth, and trihalomethane (THM) formation based on Abokifa et al. (2016) and evaluated the impact of each chemical parameter on bacterial regrowth, chlorine decay, and THM concentration. Similarly, the authors in Di Cristo et al. (2014) compared uncertainty associated with three different kinetic models for THM formation.

The sensitivity of monochloramine decay has been examined in the context of wastewater treatment plant effluent with hydraulic processes and some reactions that are specific to the river ecosystem and do not apply to WDSs (Ciffroy and Urien, 2021). In addition, the authors in Ricca et al. (2019) demonstrated that modeled monochloramine concentrations within a WDS can be reasonably approximated using field-sampling data, but did not specifically account for uncertainty associated with chemical or hydraulic influences. A literature review qualitatively describing factors influencing monochloramine decay in WDSs was performed in Li et al. (2019), however, it did not provide a quantitative tool to assess the influence of uncertain water quality parameters on monochloramine decay.

In the context of previous works, we identify three main gaps: (1) with the increase in the utilization of monochloramine by water utilities, analyzing the uncertainty related to the fate of monochloramine decay in WDSs is needed, (2) the complex water quality dynamics necessitates robust and computationally efficient uncertainty quantification methods, and (3) a unified, publicly available computational framework that can be used to assist researchers and practitioners to explore uncertainty in water quality predictions is needed.

To address these research gaps, we conduct an uncertainty characterization and propagation analysis for modeling monochoramine decay in WDSs. We characterize hydraulic uncertainty by accounting for spatial and temporal variability in water demands and chemical uncertainty by investigating the temporal variability of over 20 parameters in the monochloramine decay model. We utilize the Morris method (Saltelli et al., 2004), a global method for sensitivity analysis, to identify and quantify the impact of the influential and non-influential parameters. We then propagate uncertainty using MC simulations to quantify the contribution of hydraulic and chemical drivers by varying the influential chemical parameters identified in the previous stage. We demonstrate the results using two different WDSs supplied by gravity and pumping systems. Additionally, by decoupling the hydraulic and chemical uncertainty, we show that monochloramine decay in complex WDSs can be approximated using a simplified model (i.e., batch reactor), thus avoiding the need for detailed and calibrated water quality models, which are often unavailable for water utilities. Finally, to improve the useability of research, all codes to reproduce the chemical parameter uncertainty quantification in this work and a general template that can be used to analyze other chemical reactions and generalized to other WDSs, are made publicly available in a GitHub repository (Frankel and Sela, 2022).

2. Methods

This section describes the methods used to conduct the uncertainty analysis. First, the monochloramine decay model is presented, including the species, rate constants, and rate expressions. Next, the sources of chemical uncertainty are described, and the Morris method (Saltelli et al., 2004) and its implementation for chemical uncertainty are presented. Subsequently, the process to propagate and compare the contribution of hydraulic and chemical uncertainty to model predictions using MC simulations is described.

2.1. Chemical model

The monochloramine decay mechanisms modeled in this work include the inorganic chloramine instability and the inorganic chloramine demand attributed to reaction with total organic carbon (TOC). The model describing inorganic chloramine instability, commonly referred to as the unified model (Jafvert and Valentine, 1992), consists of 14 reactions describing the chloramine formation and decay. The reactions involving TOC, monochloramine and hypochlorous acid were developed and described in Duirk et al. (2005). Water age was also included as a modeled species within the WDS. Several simplified models of monochloramine decay have been proposed in Ozekin et al. (1996) and Roy et al. (2020), which rely on assumptions that are only valid within certain water quality ranges (Wahman, 2018). For example, the model proposed in Roy et al. (2020) was only experimentally verified for pH between 7.5–8.5. Therefore, we utilize the unified model for monochloramine decay which remains valid under a wide range of water quality conditions (Wahman, 2018).

The reactions involved in the unified model (listed in Table 1 as reactions 1–14), are comprised of four types of reactions: substitution/hydrolysis, disproportionation, redox in the absence of free chlorine, and redox in the presence of free chlorine. The unified model

Table 1
Chloramine reactions and rate expressions implemented in the reaction model (Jafvert and Valentine, 1992; Duirk et al., 2005).

Reaction number	Reaction	Rate expression	Rate constant	Value at 25 °C	Range	Reference
1	$HOCl + NH_3 \rightarrow NH_2Cl + H_2O$	$k_1[HOCl][NH_3]$	k_1	$4.2\times10^{6}\ s^{-1}$	±25%[c]	Morris and Isaac (1983)
2	$NH_2Cl + H_2O \rightarrow HOCl + NH_3$	$k_2[NH_2Cl]$	k_2	$2.1\times10^{-5}\ s^{-1}$	±25%[d]	Morris and Isaac (1983)
3	$HOCl + NH_2Cl \rightarrow NHCl_2 + H_2O$	$k_3[HOCl][NH_2Cl]$	k_3	$280\ s^{-1}$	±25%[d]	Morris and Isaac (1983)
4	$NHCl_2 + H_2O \rightarrow HOCl + NH_2Cl$	$k_4[NHCl_2]$	k_4	$6.5\times10^{-7}\ s^{-1}$	±25%[d]	Margerum et al. (1978)
5[a]	$NH_2Cl + NH_2Cl \rightarrow NHCl_2 + NH_3$	$k_5[NH_2Cl]^2$	k_{5H}	$6.9\times10^{3}\ M^{-2}s^{-1}$	±25%[d]	Granstrom (1955)
			k_{5HCO_3}	$2.2\times10^{-1}\ M^{-2}s^{-1}$	±25%[d]	Peter et al. (2001)
			$k_{5H_2CO_3}$	$11\ M^{-2}s^{-1}$	±25%[d]	Peter et al. (2001)
6	$NHCl_2 + NH_3 \rightarrow NH_2Cl + NH_2Cl$	$k_6[NHCl_2][NH_3][H^+]$	k_6	$6.0\times10^{4}\ M^{-2}s^{-1}$	±25%[d]	Hand and Margerum (1983)
7[e]	$NHCl_2 + H_2O \rightarrow I$	$k_7[NHCl_2][OH^-]$	k_7	$110\ M^{-1}s^{-1}$	±25%[d]	Jafvert and Valentine (1987), Jafvert (1985)
8[e]	$I + NHCl_2 \rightarrow HOCl + N_2 + 3H^+ + 3Cl^-$	$k_8[I][NHCl_2]$	k_8	$2.8\times10^{4}\ M^{-1}s^{-1}$	±25%[d]	Leao (1981)
9[e]	$I + NH_2Cl \rightarrow N_2 + 3H^+ + 3Cl^-$	$k_9[I][NH_2Cl]$	k_9	$8.3\times10^{3}\ M^{-1}s^{-1}$	±25%[d]	Leao (1981)
10	$NH_2Cl + NHCl_2 \rightarrow N_2 + 3H^+ + 3Cl^-$	$k_{10}[NH_2Cl][NHCl_2]$	k_{10}	$1.5\times10^{-2}\ M^{-1}s^{-1}$	±25%[d]	Leao (1981)
11[b]	$HOCl + NHCl_2 \rightarrow NCl_3 + H_2O$	$k_{11}[HOCl][NHCl_2]$	k_{11CO_3}	$6.0\times10^{6}\ M^{-2}s^{-1}$	±33%[c]	Hand and Margerum (1983)
			k_{11OCl}	$9.0\times10^{4}\ M^{-2}s^{-1}$	±44%[c]	Hand and Margerum (1983)
			k_{11OH}	$3.28\times10^{9}\ M^{-2}s^{-1}$	±3%[c]	Hand and Margerum (1983)
12	$NHCl_2 + NCl_3 + 2H_2O \rightarrow N_2 + 2HOCl + 3HCl$	$k_{12}[NHCl_2][NCl_3][OH^-]$	k_{12}	$5.56\times10^{10}\ M^{-2}s^{-1}$	±25%[d]	Jafvert and Valentine (1992)
13	$NHCl_2 + NCl_3 + H_2O \rightarrow N_2 + HOCl + 3HCl$	$k_{13}[NH_2Cl][NCl_3][OH^-]$	k_{13}	$1.39\times10^{9}\ M^{-2}s^{-1}$	±25%[d]	Jafvert and Valentine (1992)
14	$NHCl_2 + 2HOCl + H_2O \rightarrow NO_3^- + 5H^+ + 4Cl^-$	$k_{14}[NHCl_2][OCl^-]$	k_{14}	$231\ M^{-1}s^{-1}$	±25%[d]	Jafvert and Valentine (1992)
15	$NH_2Cl + DOC_1 \rightarrow NH_3 + Products$	$k_{DOC_1}[NH_2Cl][DOC_1]$	k_{DOC_1}	$5.4\ M^{-1}s^{-1}$	±55%[c]	Duirk et al. (2005)
16	$HOCl + DOC_2 \rightarrow Products$	$k_{DOC_2}[HOCl][DOC_2]$	k_{DOC_2}	$180\ M^{-1}s^{-1}$	±10%[c]	Duirk et al. (2005)
17	AGE	1	–	–	–	–

[a] $k_5 = k_{5H}[H^+] + k_{5HCO_3}[HCO_3^-] + k_{5H_2CO_3}[H_2CO_3]$.

[b] $k_{11} = k_{11CO_3}[CO_3^{2-}] + k_{11OCl}[OCl^-] + k_{11OH}[OH^-]$.

[c] Uncertainty range cited or inferred from literature.

[d] Uncertainty range not reported, range is assumed.

[e] I is an unidentified intermediate species.

Table 2
Equilibrium reactions and constants.

Reaction number	Reaction	Equilibrium constant at 25 °C	Reference
17	$HOCl \rightleftharpoons H^+ + OCl^-$	2.79×10^{-8}	Morris (1966)
18	$NH_4^+ \rightleftharpoons NH_3 + H^+$	5.05×10^{-10}	Bates and Pinching (1950)
19	$H_2CO_3 \rightleftharpoons HCO_3^- + H^+$	4.37×10^{-7}	Snoeyink and Jenkins (1980)
20	$HCO_3^- \rightleftharpoons CO_3^{2-} + H^+$	4.40×10^{-11}	Snoeyink and Jenkins (1980)
21	$H_2O \rightleftharpoons OH^- + H^+$	1.09×10^{-14}	Snoeyink and Jenkins (1980)

also includes equilibrium reactions between free chlorine, ammonia, and carbonate species (listed in Table 2). Table 1 lists the values of the rate constants reported in the literature and the associated uncertainty range (described further in Section 2.2.1). Additional details on the unified model can be found in Jafvert and Valentine (1992).

Oxidation of TOC by monochloramine was modeled using the two reaction pathways described in Duirk et al. (2005), represented by reactions 15 and 16 in Table 1. The first pathway involves the oxidation of TOC by monochloramine, while the second pathway involves the oxidation of TOC by hypochlorous acid (HOCl) formed as a result of monochloramine hydrolysis. The first pathway occurs at a much higher rate than the second pathway (Duirk et al., 2005). Reactions 15 and 16 include species DOC_1 and DOC_2 that represent the overall fraction of TOC, which is active for each reaction pathway. Additional parameters, S_1 and S_2, represent the fraction of TOC involved in each reaction pathway (see Table 3), and are used to calculate the initial concentration of DOC_1, i.e. $S_1 \times$ TOC and the initial concentration of DOC_2, i.e, $S_2 \times$ TOC.

We note important properties of the rate of monochloramine decay (see Fig. 1). We use a simplified model, i.e., the batch reactor model, to simulate the dynamics of the chemical reactions without the effect of hydraulic conditions within a complex network of pipes in the WDS. As seen in Fig. 1, there is an initial rapid decrease in monochloramine concentration, followed by a prolonged decrease at a slower rate. Though all reactions are occurring simultaneously, the initial rapid decline in monochloramine concentration is a result of the oxidation of DOC_1 by monochloramine. After the concentration of DOC_1 has been depleted, the oxidation of DOC_2 forms hypochlorus acid, and

Table 3
Initial species concentrations, selected to represent the composure of a hypothetical drinking water treatment plant effluent.

Parameter	Value	Range
pH	7–9.5	Varies[a]
TOTNH	$0.15\ \frac{mg}{l}$ as N	±25%
TOTCO	$200\ \frac{mg}{l}$ as $CaCO_3$	±25%
TOC	$1.5\ \frac{mg}{l}$	±25%
S_1	0.016	±40%[b]
S_2	0.57	±24%[b]

[a] Additional information on the pH used in each simulation detailed in Section 3.2.2.

[b] Uncertainty range inferred from Duirk et al. (2005); TOTNH refers to initial concentration of total ammonia; TOTCO refers to initial concentration of total carbonate; TOC refers to initial concentration of total organic carbon.

the additional reactions in the unified model continue. The magnitude of the initial drop in monochloramine concentration is approximately equal to the initial concentration of DOC_1, since there is a one-to-one stoichometric ratio in the reaction between monochloramine and DOC_1. The dynamics of the rate of monochloramine decay as a result of the two different pathways is relevant to our discussion of influential chemical parameters in Section 3.2. In addition, we use Fig. 1 to demonstrate the difference between chemical and hydraulic uncertainty, discussed further in Section 2.3. Hydraulic uncertainty refers to uncertainty in water age observed at a particular location in a WDS, while chemical uncertainty refers to uncertainty in the modeled concentration of monochloramine at a specific water age.

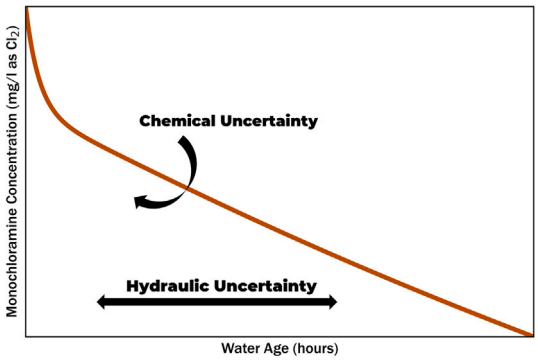

Fig. 1. Example of monochloramine decay in a batch reactor.

2.2. Characterizing chemical uncertainty

The first step in the uncertainty analysis is to determine the sensitivity of the rate of monochloramine decay based on each chemical parameter listed in Table 1. The purpose of this analysis is two-fold. First, having insight to the most influential parameters is useful to prioritize which chemical parameters should be experimentally verified or adjusted for a specific water source. Second, identification of non-influential parameters allows for those parameters to be held constant since they do not affect model predictions, thus reducing the dimensionality of the problem. The Morris method, which has been demonstrated to be robust and computationally efficient, was used estimate the sensitivity in model predictions associated with uncertainty in chemical parameters (Yang, 2011; Herman et al., 2013; Saltelli et al., 2004). The Morris method involves iteratively changing input parameters one-at-a-time to quantify the influence of each input parameter on model output, and provides similar insights to more computationally expensive methods (e.g., Sobol method) (Herman et al., 2013; Silva and Ghisi, 2020; Pannier et al., 2018). The Morris method is a global sensitivity method, which yields two metrics for each parameter: μ^*, which indicates the level of influence of each parameter, and σ, which indicates the level of interaction with other parameters. In our context, the Morris method provides a good compromise between accuracy and computational efficiency.

Executing the Morris method involves the following main steps: (1) For each k uncertain parameters, a range of possible parameter values is defined. (2) The range of each parameter is divided into equal size intervals, yielding a k-dimensional grid (Ω) representing the parameter space. (3) Initial parameter values are assigned by selecting a coordinate (randomly according to a uniform distribution) within Ω, and the model is evaluated. (4) k additional model evaluations are conducted, where for each successive model evaluation one of the k parameters is modified to a different value within Ω. The process of defining initial parameter values and iteratively conducting $k+1$ model evaluations (steps 3 and 4) is defined as a *trajectory*. (5) In order to evaluate the overall influence of each parameter over its entire range and level of interaction with other parameters, r trajectories are conducted, requiring a total of $r(k+1)$ model evaluations. (6) After all model evaluations are completed, the elementary effect of each uncertain input parameter is computed based on the change in model output in response to the change in each uncertain input parameter. Then, the absolute mean (μ^*) and standard deviation (σ) of the elementary effects are computed to quantify the influence of each uncertain input model parameter.

Specifically, for each input parameter, $(x_1, \ldots, x_i, \ldots, x_k)$, a lower bound, L_i, and upper bound U_i is defined. The parameter space Ω is a k-dimensional grid, with bounds 0 and 1, representing the normalized values between L_i and U_i along each dimension. The grid is then discretized into p-levels, with $p-1$ cells in each dimension. Intuitively, the hyper-parameter p defines the resolution of the grid. For example, if a parameter x_i has a defined range between 0 and 1, and $p = 4$ (i.e., 4 points and 3 intervals), then the size of each cell is $\frac{1}{4-1} = 0.33$. An additional hyper-parameter δ, which defines the size of the perturbation or change in the value of each uncertain parameter, is selected. For example, if $p = 4$ and $\delta = \frac{2}{3}$, we will move two cells when changing the model parameter. Saltelli et al. (2004) showed that selecting values of 4 and $\frac{2}{3}$ for the values of p and δ, respectively, are desirable for coverage of the entire range of possible parameter values.

We now describe how the values of μ^* and σ are calculated, and formally define the term elementary effect. In essence, an elementary effect is the change in model output as a result of changing a model parameter as described previously. The elementary effect of parameter x_i and trajectory j (d_{ji}) is defined as:

$$d_{ji} = \frac{f(x_1, \ldots, x_i + \delta, \ldots, x_k) - f(x_1, \ldots, x_i, \ldots, x_k)}{\delta} \quad (1)$$

where f is the model output. The metric μ_i^* is the mean of the absolute values of the elementary effects in the set $(d_{1i}, \ldots, d_{ji}, \ldots, d_{ri})$ and indicates the influence of parameter x_i. The metric σ_i is the standard deviation of the elementary effects of parameter x_i, which indicates the level of interaction between x_i and the other parameters. Conducting additional trajectories increases the combinations of model input parameters, allowing for increased coverage of the overall parameter space to be reflected in the calculated values of μ^* and σ. Additional details on the Morris method can be found in Saltelli et al. (2004), and an example implementation can be found in the Supporting Information (SI).

2.2.1. Application to monochloramine decay

The Morris method was applied to the monochloramine decay model to determine the sensitivity of model predictions to each model parameter as a function of time. The concentration of monochloramine at time t is defined as $c(x,t)$. Parameter set x consists of rate constants in the monochloramine reaction model, initial concentrations of total organic carbon (TOC), total ammonia (TOTNH), and total carbonate (TOTCO), and the fraction of TOC involved in the fast (S_1) and slow (S_2) reactions with monochloramine and hypochlorus acid. The bounds for each parameter, shown in Tables 1 and 3, were estimated from literature values of each parameter. In some instances, a range of uncertainty for a parameter is noted. For example, Morris and Isaac (1983) specifically notes that based on the underlying experimental data, the uncertainty surrounding rate constant k_1 is ±25%. In other instances, no uncertainty bound for a parameter was reported in the literature, and a range of ±25% from the nominal value was used in lieu of a specified uncertainty range. In order to evaluate the sensitivity of each parameter as a function of time, i.e., water age, values of μ_i^* and σ_i were calculated for all timesteps of each model evaluation.

In the implemented monochloramine model, the pH is not affected by the reactions involving monochloramine decay. Yet, pH affects the reaction dynamics since the disproportionation of monochloramine (reaction 5 in Table 1) is acid-catalyzed, and speciation between acid and conjugate base species (ammonia, carbonate, and free chlorine) affects reaction kinetics. In order to illuminate the interaction between pH and each parameter, the Morris method analysis was repeated for values of pH between 7.0 and 9.5 (representing pH of various WDSs) with increments of 0.5, and at pH 7.75, for a total of 7 repetitions. The initial concentration of monochloramine of the finished water at the treatment plant was held constant at 3.0 mg/l as Cl_2, representing a typical value of finished water monochloraine concentration within major water utilities in the State of Texas (Houston Public Works, 2021; Dallas Water Utilities, 2021; Austin Water Utility, 2021), and was not treated as a source of uncertainty in this study. For all model evaluations, temperature was held constant at 25°C, representing typical conditions within a WDS (Agudelo-Vera et al., 2020; Pfaller et al., 2021).

2.3. Characterizing hydraulic uncertainty

In this section, we conceptually demonstrate the difference between chemical and hydraulic uncertainty, characterize the source of hydraulic uncertainty used in this study, and then describe how we propagated hydraulic uncertainty to quantify the impact to monochloramine concentrations.

Water quality in a WDS is mainly governed by transport (or advection) and chemical reactions, with minimal impact from diffusion and dispersion (Abokifa et al., 2016). We return to Fig. 1 to differentiate between chemical and hydraulic uncertainty. Chemical uncertainty affects the rate of a chemical reaction, leading to uncertainty in the concentration of a chemical concentration at any given water age. On the other hand, hydraulic uncertainty ultimately results in variation of velocities within a WDS (and therefore water age), describing the amount of time that a chemical reaction is able to occur while the water travels from a treatment plant to a consumer at a specific location in the system. The batch reactor model (illustrated in Fig. 1) will be used in Section 3.3.2 to demonstrate how the propagation of uncertainty affects monochloramine concentrations at different locations within a WDS. To quantify the effect of uncertain hydraulic conditions in a WDS, and the subsequent contribution to water quality variability, we use the metric of water age.

We consider the variability in consumer demands as the source of hydraulic uncertainty, since it has been demonstrated to be a significant source contributing to the variability in water quality within a WDS (Hatam et al., 2021; Zhuang and Sela, 2020). For a given WDS, we first classify each demand node into a particular consumer class (i.e., residential, commercial, or mixed-use). Next, uncertainty in user demand is modeled using a multivariate normal (MVN) distribution, which is parameterized by mean vector and correlation matrix (Tong, 2012). Using a MVN distribution accounts for correlations between demands among user groups, enabling simulation of realistic cases in which user demands are correlated. For example, positive correlation between user groups could represent a scenario in which residential and mixed-use demands increase during peak hours and decrease during off peak hours according to a similar pattern. Similarly, negative correlation could represent a scenario simulating the effects of social distancing policies (e.g., during COVID-19 pandemic), resulting in an increase in residential demand, but a decrease commercial demand (Spearing et al., 2021).

2.4. Propagating chemical and hydraulic uncertainty

We now seek to propagate chemical and hydraulic uncertainty within a WDS using MC simulations and compare the overall effects of uncertainty in chemical parameters with the uncertainty in hydraulic conditions. Three different demand scenarios were considered, each with different correlation structure. To account for chemical uncertainty, the influential parameters identified using the Morris method were varied, and parameters shown to be non-influential remained constant. For the MC simulations in which chemical parameters were varied, a uniform distribution was assumed between the lower and upper bound specified in Tables 1 and 3. Chemical parameter values were generated using Latin Hypercube sampling to maximize coverage of the parameter space while constraining the number of evaluations (Mckay et al., 1979). Finally, scenarios accounting for joint chemical and hydraulic uncertainty were also evaluated. Overall, seven different scenarios were evaluated (as described in Section 3.3). Results of the MC simulations were summarized qualitatively and quantitatively using different summary statistics (e.g., mean, standard deviation, percentiles, and histograms) and used to evaluate the temporal and spatial variability in monochloramine concentrations and water age at each location in the WDSs.

2.5. Software

All hydraulic and chemical simulations were conducted using EPANET-MSX, a publicly available software for simulating multi-species chemical reactions within WDSs (Shang et al., 2008). Python was used to interact with the EPNAET-MSX programmer's toolkit functions, set up the simulations, pre- and post-process results. The results of our monochloramine decay model implemented in EPANET-MSX were validated by comparing model results with (Wahman and Speitel, 2012; Wahman, 2018) to ensure no inadvertent errors. The Morris method was implemented using the SALib python package (Iwanaga et al., 2022; Herman and Usher, 2017). Model evaluations were run on the Stampede2 cluster at the Texas Advanced Super Computer at the University of Texas (TACC - Texas Advanced Computing Center, 2020). The codes used to set up the multi-species reaction model in WDSs and execute the chemical uncertainty analysis are publicly available in GitHub repository (Frankel and Sela, 2022). The codes can be seamlessly generalized to be applied towards different reaction schemes (including species attached to a pipe wall) and other WDSs.

3. Results

3.1. Description of the water systems

The proposed methodology was tested and applied towards three water systems, each with increasing complexity, as follows: (1) *Water System 1 (WS1)* – is a batch reactor used to simulate the dynamics of the chemical reactions without the influence of hydraulic conditions within a WDS. (2) *Water system 2 (WS2)* – is adopted from (Ormsbee et al., 2022) (commonly referred to as PA2). WS2 represents part of a distribution system in Harrisburg, PA. The hydraulic model of WS2 consists of 288 pipes and 263 nodes (a node in the model represents a cross connection between different pipes and/or a consumer), with a total daily demand of approximately 4163 cubic meters per day. The system is supplied by gravity, has one water source, and no storage tanks. The mean water age in the network is 17 h. A schematic of WS2, including the demand at each node, is shown in Figure S1a in the SI. Additional details can be found in Ormsbee et al. (2022). (3) *Water system 3 (WS3)* – is adopted from (Ormsbee et al., 2022) (commonly referred to as Net3). WS3 is based on the North Marin Water District in Novato, CA. The hydraulic model of WS3 consists of 117 pipes and 97 nodes, and total demand of approximately 18,549 cubic meters per day. There are two sources of water, two pumping stations, and three storage tanks within the network. The mean water age of the network is 25 h, however, water age can reach 150 h in certain nodes as a result of water held in a storage tank and subsequently routed to a demand node. A schematic of WS3, including the demand at each node, is shown in Figure S1b in the SI. Additional details can be found in Ormsbee et al. (2022).

The simulation duration for WS1 was 7 days, and the entire period was used for the Morris method. When conducting model evaluations for WS2 or WS3 using the MC method, the simulations were performed for an extended duration to allow the chemical concentrations within the network to reach a steady state, which was 10 and 18 days, respectively. The results of the final 24-h period in WS2 and WS3 were used for analysis.

3.2. Chemical uncertainty analysis

Our first objective is to identify the influential and non-influential chemical parameters governing monochloramine decay and track the evolution of the uncertainty in time. In order to maximize coverage of the input parameter space while keeping the number of model evaluations relatively low, the method developed in Ruano et al. (2012) was implemented, in which m potential trajectories are randomly generated, and then the most disparate r trajectories are selected for model

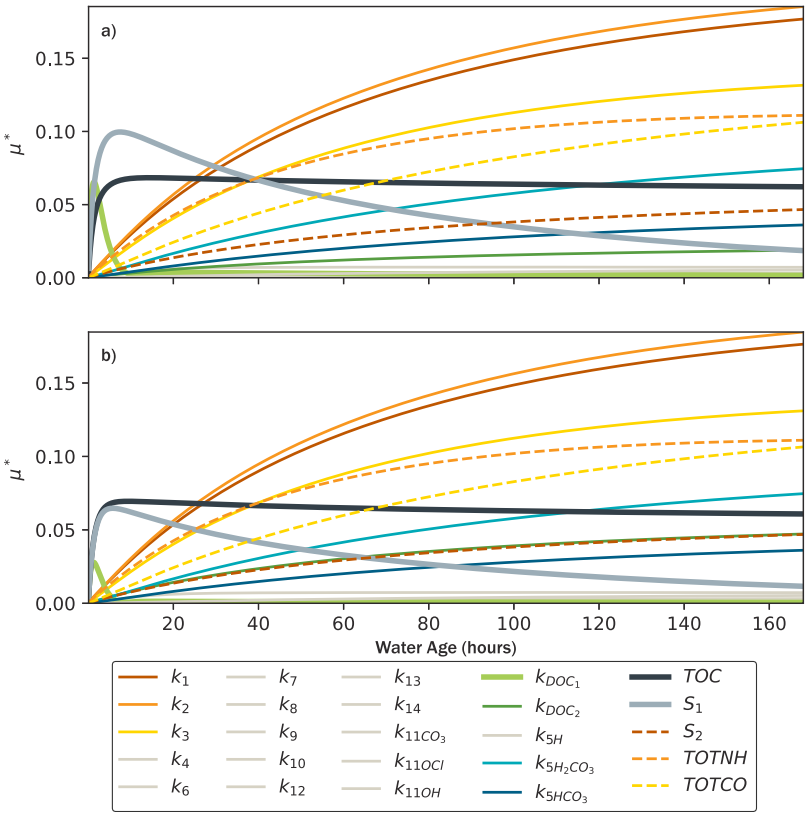

Fig. 2. Results of the Morris method applied to WS1 at pH 7.75. (a) Parameter-specific uncertainty range, as shown in Tables 1 and 3. (b) All parameter uncertainty ranges fixed at ±25%. Non-influential parameters are shown with thin gray lines.

evaluations. In our implementation, the values of m and r were selected as 1000 and 10, respectively. To track the evolution of uncertainty with time, the duration of each simulation was 7 days with 5-min timestep, and μ^* and σ were evaluated at every timestep. The values of μ^* for each parameter as a function of time, indicating the influence of each parameter on the concentration of monochloramine at each timestep, are shown in Fig. 2a.

Fig. 2a shows a clear delineation between influential and non-influential parameters. The non-influential parameters maintain values of μ^* below 0.001 for the entire duration of the simulation (shown with thin gray lines), contrasted with the parameters for which the values of μ^* are relatively higher. Among the influential parameters, Fig. 2a reveals two main trends in parameter sensitivity. Parameters $kDOC_1$, S_1 and TOC exhibit greatest values of μ^* at water ages less than 10 h and then wane, while the value of μ^* for other parameters steadily increases with water age. The initial increase in the values of μ^* exhibited by parameters $kDOC_1$, S_1 and TOC is due to the parameters effect on the fast initial decay in monochloramine decay (as described in Section 2.1). The product of TOC and S_1 represent the initial concentration of DOC_1, which is approximately equal to the magnitude of the initial drop in monochloramine concentration as a result of the fast monochloramine-TOC reaction pathway (reaction 15 in Table 1). After all of the DOC_1 has been oxidized by monochloramine at approximately 10 h, the reaction ceases and the value of $kDOC_1$ is inconsequential for the remaining reaction. The value of μ^* for TOC wanes throughout the remainder of the simulation, but remains high due to its participation in the slow-reaction pathway with monochloramine (reaction 16 in Table 1). The remaining influential parameters consist of parameters involved in the unified model and slow reaction pathway between monochloramine and TOC. The influential parameters are (in order of descending value of μ^* at water age of 7 days): k_1, k_2, k_3, TOTNH, TOTCO, $k_{5H_2CO_3}$, k_{DOC_2}, and S_2.

3.2.1. Impact of parameter uncertainty range

In order to differentiate between the effect of input parameter range, and the effect of the parameter itself, the analysis was repeated with uncertainty ranges for all parameters of ±25%. Fig. 2a shows the results with parameter uncertainty ranges according to Tables 1 and 3, while Fig. 2b shows the results with all parameter ranges at ±25%. The difference between Fig. 2a and Fig. 2b illuminates the effect of the parameter input uncertainty ranges. The main effect is observed in the values of μ^* for parameters S_1 (thick gray), TOC (black), and k_{DOC1} (green). The rate expression for the fast-reaction pathway of TOC is $k_{DOC1}[NH_2Cl][DOC_1]$, where the initial concentration of DOC_1 = TOC × S_1. Therefore, it follows that when S_1, TOC, and k_{DOC1} all exhibit uncertainty of ±25%, S_1 and TOC have equal values of μ^* (while the fast-reaction pathway is active), since the product of the two parameters have equal effect in determining the initial concentration of DOC_1, as shown in Fig. 2b. However, data from (Duirk et al., 2005) suggests that the uncertainty bounds on k_{DOC1} and S_1 are ±55% and ±40%, respectively, while TOC was assumed to remain at ±25%. Therefore, the increased uncertainty attributed to higher peak values of μ^* for parameters k_{DOC_1} and S_1, is shown in Fig. 2a. This demonstrates that the range of uncertainty assigned to a particular parameter contributes to its reported level of influence in the Morris method (via the values of μ^* and σ), and that to the extent possible, modelers should take care to accurately characterize parameter uncertainty ranges.

In addition to evaluating the level of influence of each parameter indicated by μ^*, the level of interaction between each parameter and all other parameters, indicated by σ, also conveys valuable insights. Figure S2 in the SI shows the values of σ for each timestep. Figure S2 demonstrates that the relative level of interaction of each parameter with other parameters generally aligns with its level of influence (μ^*). In addition, multiple parameters exhibit interactions, giving creedence to our approach for sampling from a range of all influential parameters to capture the effects of the interactions.

Table 4
Mean values of the base demand factor for each scenario.

Scenario	Residential	Commercial	Mixed use
Hyd1	1	1	1
Hyd2	0.7	1	1.3
Hyd3	1.3	0.75	1.2

Table 5
Correlation matrix between user groups.

Scenario	C_{rc}	C_{rm}	C_{cm}
Hyd1	0	0	0
Hyd2	−0.5	0.6	−0.3
Hyd3	0.4	0.0	0.0

C_{rc}: residential and commercial user groups; C_{rm}: residential and mixed use user groups; C_{cm}: commercial and mixed use user groups.

Table 6
Mean and standard deviation (std) of monochloramine concentrations (mg/l as Cl_2).

Scenario	WS2	WS3
	Mean (std)	Mean (std)
Chem	2.70 (0.20)	2.76 (0.13)
Hyd1	2.70 (0.21)	2.76 (0.11)
Hyd1-Chem	2.70 (0.22)	2.76 (0.12)
Hyd2	2.72 (0.21)	2.76 (0.11)
Hyd2-Chem	2.72 (0.22)	2.76 (0.12)
Hyd3	2.72 (0.24)	2.75 (0.18)
Hy3d-Chem	2.72 (0.24)	2.75 (0.19)

3.2.2. Impact of pH

pH is an important factor in the rate of monochloramine decay, as it controls the ratio of ammonia, carbonate, and free chlorine species between each acid/conjugate base pair. In addition, the disproportionation of monochloramine (reaction 5 in Table 1), which is the rate-controlling reaction for monochloramine decay, is acid-catalyzed (Jafvert and Valentine, 1992). Therefore, the rate of monochloramine decay increases as pH decreases (i.e. the water increases in acidity). Figure S3 in the SI shows the difference in monochloramine decay at values of pH 7.0–9.5, demonstrating that the rate of monochloramine decay attributed to the unified model increases as pH decreases (as is expected given the acid-catalyzed nature of monochloramine decay); however, the initial drop in monochloramine decay attributed to the fast reaction pathway with TOC is the same for all pH levels. Therefore, the Morris method was repeated for WS1, in which the pH was varied between 7 and 9.5 to assess how the values of μ^* vary at different pH levels (see Figures S4-S12 in the SI). Comparison of the values of μ^* reveals multiple trends in parameter sensitivity. First, although the fast reaction pathway of TOC oxidation is not chemically affected by pH, the influence of S_1 (measured by the value of μ^*) increases. This is because as pH increases, the decay attributed to the unified model decreases, and the initial drop in monochloramine has a larger overall influence on monochloramine concentration throughout the duration of the simulation. Similarly, for $k_{5H_2CO_3}$, as pH increases, the rate of decay of monochloramine decreases as a result of the unified model and slow reaction pathway with TOC (reactions 1–14 and 16 in Table 1). As a result, the value of μ^* for each parameter (except for $k_{5H_2CO_3}$) decreases with increasing pH. The increase in values of μ^* for $k_{5H_2CO_3}$ with increasing pH is attributed to its role in catalyzing the disproportionation of monochloramine (reaction 5 in Table 1). Since the concentrations of H_2CO_3 and H^+, by definition, decrease with increasing pH, the proportion of influence of the overall value of k_5 is attributed to $k_{5H_2CO_3}$ and TOTCO.

3.3. Comparison of hydraulic and chemical uncertainty

The contribution of chemical and hydraulic uncertainty to uncertainty in monochloramine predictions was evaluated and compared for different scenarios using MC simulations. The distribution of monochloramine concentration over a 24-h simulation period at each node were compared to assess the overall sensitivity to chemical and hydraulic factors. For each scenario, 150 hydraulic model evaluations were conducted, which was sufficient to achieve stable mean and characterize the expected distribution of monochloramine concentrations.

The chemical parameters found to be influential were sampled from uniform distribution using Latin Hypercube sampling scheme (Mckay et al., 1979), with the upper and lower bounds of each parameter specified in Tables 1 and 3. To propagate hydraulic uncertainty, the nodes in WS2 and WS3 were classified into one of three user groups: residential, commercial, and mixed use. The user groups associated with each node are shown in Figure S13 in the SI. Three scenarios were considered with different hydraulic uncertainty. In each scenario, demands were varied by scaling the base demand at each node based on MVN. For each scenario, each user group was assigned a scaling factor with mean and correlation shown in Tables 4 and 5, with a standard deviation of 0.1. For example, scenario Hyd1 represents the underlying uncertainty and variability of normal WDS operations. Scenarios Hyd2 and Hyd3 represent group-wide shifts in water usage, with different correlation structure. Scenario Hyd3 is based on the correlation observed among different users based on data collected at the University of Texas at Austin and analyzed in Frankel et al. (2021). In addition, for each of the three hydraulic scenarios, MC simulations were executed again varying the hydraulic and chemical conditions simultaneously. Overall, seven scenarios were considered: Chem – considering only chemical uncertainty; Hyd1, Hyd2, Hyd3 – three demand scenarios; and Hyd1-Chem, Hyd2-Chem, Hyd3-Chem – joint demand and chemical scenarios.

3.3.1. System-wide analysis

Fig. 3 shows the mean monochloramine concentration for WS2 and WS3 for scenario Hyd1-Chem, where the color of each marker represents the mean and the size the standard deviation of the monochloramine concentration at each node. Fig. 3 shows that most nodes in both networks have mean monochloramine concentrations near 2.75 mg/l as Cl_2, and that nodes with lower mean monochloramine concentration also exhibit greater standard deviations (the relationship between low concentration and higher variability in monochloramine concentration is further explained in 3.3.3). Similar system-wide results were obtained for the other uncertainty scenarios. Table 6 shows the mean and standard deviation for all nodes for each scenario for WS2 and WS3. We observe that for each system all scenarios result in similar mean and standard deviation of monochloramine concentration. Hence, based on the system-wide results alone, for the systems utilized in this study, it is inconclusive whether hydraulic or chemical uncertainty is a greater driver of overall monochloramine uncertainty at each location within the WDSs. However, we garner insights into this question by further observing the dynamics of individual locations in the WDSs.

3.3.2. Location-specific analysis

We use node 141 in WS3 (see Fig. 3) to demonstrate the relationship between water age, hydraulic uncertainty, and chemical uncertainty. Fig. 4 shows the modeled water age and monochloramine concentration over 24 h. Fig. 4a shows the water age profile under the baseline demand conditions (i.e., no hydraulic uncertainty) with chemical uncertainty (i.e., scenario Chem). Similarly, Fig. 4b shows the water age profiles in the same node considering also hydraulic uncertainty (i.e., scenario Hyd1-Chem). Fig. 4c and d show the distribution of monochloramine concentrations at each timestep for the same scenarios, Chem and Hyd1-Chem, respectively. At each timestep, the different colors represent different percentiles: 0-25% (blue), 25-50% (green), 50-75% (yellow), and 75-100% (orange).

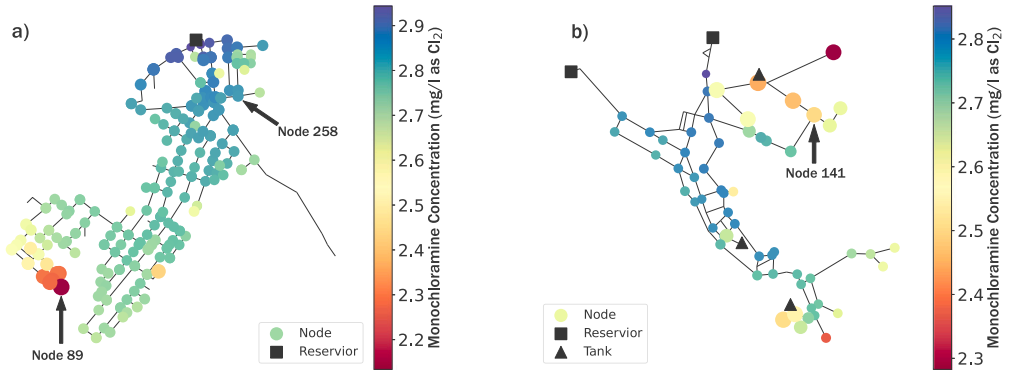

Fig. 3. Mean monochloramine concentrations for scenario Hyd1-Chem: (a) WS2 and (b) WS3.

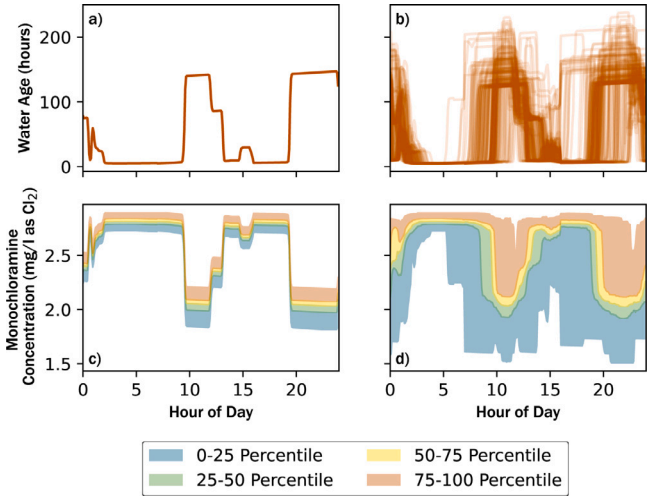

Fig. 4. Results at node 141 in WS3: (a) predicted water age with chemical uncertainty, (b) predicted water age with chemical and hydraulic uncertainty, (c) predicted monochloramine concentrations with chemical uncertainty, (d) predicted monochloramine concentrations with chemical and hydraulic uncertainty.

Fig. 4a shows that there is an abrupt variability in the water age at the given location. For example, during simulation hours 3–9, water age is approximately 5 h, and during simulation hours 10–12, water age significantly increases to 140 h. This is a result of the specific system dynamics, such that the water age is relatively low when water is supplied directly from the source, which is characterized by shorter travel times, compared to higher water ages when water is supplied from the storage tanks. Fig. 4b shows that when hydraulic uncertainty is introduced, there is variability in predicted water age (i.e., output uncertainty). In this network, the main driver of water age variability is related to the dynamics of the tanks in relation to changing demands. The stochastic water demands within the network manifest in varied times in which node 141 is supplied directly from the source versus from water in the tank. For example, at simulation hour 4, for all 150 simulations, water age is approximately 5 h because water is supplied directly from the source. However, at nearly all other times in the simulation, variability in water age at node 141 is attributed to whether or not water is supplied directly from the source or from a tank, and the equilibrium water age within the tank.

There are multiple pertinent observations regarding the uncertainty of monochloramine concentration with respect to water age. First, there is greater distribution in monochloramine concentration at times when water ages are higher. Considering only chemical uncertainty (scenario Chem), the distribution of monochloramine concentrations at relatively high water ages (e.g., water age of 145 h at hour 22) reveals higher output uncertainty compared to lower water ages (e.g., water age of 8 h at hour 5), see Fig. 4(c). Second, including hydraulic uncertainty introduces significant variability in water age, and in turn, in monochloramine concentrations (see Fig. 4d). Third, comparing Figures Fig. 4(c) and Fig. 4(d) shows the effect of hydraulic uncertainty on the monochloramine concentrations. Including hydraulic uncertainty increases temporal variability in monochloraine concentration, which has implications for sampling protocols. For example, at time 17 h, if only considering chemical uncertainty, the monochloramine concentration is expected to be between approximately 2.70 and 2.85 mg/l, but ranges between approximately 1.70 to 2.85 mg/l when considering hydraulic and chemical uncertainty. Similar results are shown for node 89 in WS2 in Figure S14 in the SI, however, because WS2 is supplied directly from the source and does not utilize storage tanks, the abrupt changes in water age (and therefore monochmoramine concentration) are not observed in WS2. Finally, since most nodes within WS3 are supplied with water directly from the sources and not from the tanks, the aggregated mean and standard deviation of monochloramine concentration for the entire network (shown in Table 6) masks the important water quality implications at specific nodes within the WDS.

Fig. 5 further demonstrates the variability in monochloramine concentrations throughout the course of a day for selected nodes in WS2 (top) and WS3 (bottom). The hourly mean monochloramine concentration is represented by color of each dot, and the hourly standard deviation is represented by the size of each dot. As seen in Fig. 5, each node varies in regards to its daily monochloramine concentration profile. For WS2, standard deviation and mean concentration are consistent for each node throughout a day. However, for WS3, there is greater variability in the monochloramine concentrations among nodes, and the time of day in which monochloramine concentrations vary is different between nodes. For example, in WS3, Node 253 experiences greatest variability and lowest concentrations between hours 0–5, and much higher concentration with low variability throughout the rest of the day. In contrast, Node 131 in WS3 experiences greater variability throughout the course of the day, with lower concentrations between hours 9–11 and 18–23. As previously demonstrated for node 141 in WS3, the tanks and the specific hydraulic conditions impact water trajectory (i.e., directly from the source or passed through storage tanks) and greatly affect the monochloramine concentrations. Nodes 197, 121 and 101 are all in close proximity and are directly supplied by the sources, leading to higher monochloramine concentrations and low variability. On the other hand, nodes 131, 179, 139, and 253 receive water from storage tanks during parts of the day, resulting in decreased monochloramine concentrations and higher variability. For comparison, Figure S15 in the SI shows the average fraction of water that was supplied by the tanks in WS3. The analysis shown in Fig. 5 provides a concise summary of the temporal variability in monochloramine concentrations, which can be used to identify times of greater uncertainty.

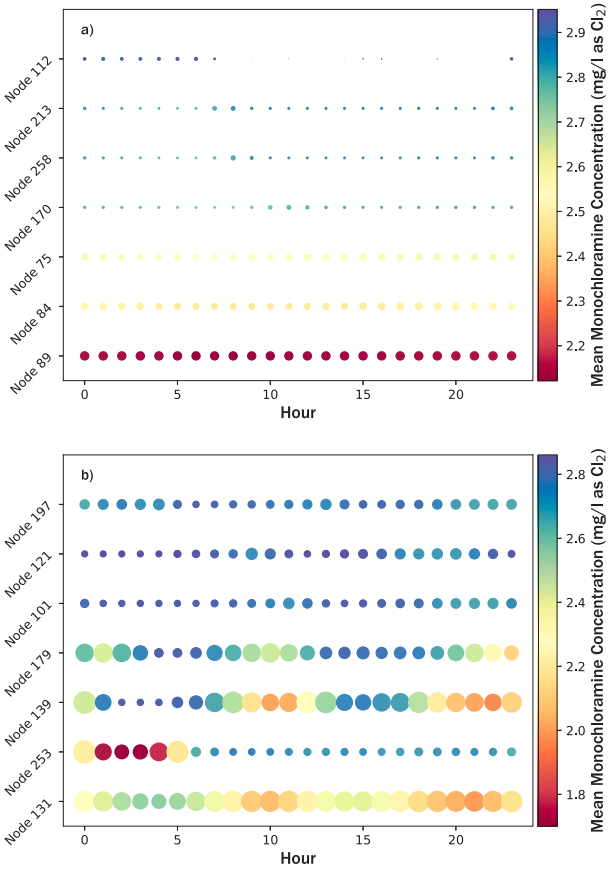

Fig. 5. Dot heat map showing hourly mean and standard deviation of monochloramine concentration at selected nodes for: (a) WS2 and (b) WS3. Dot color represents mean concentration and size represents standard deviation.

3.3.3. *Estimating output uncertainty using the batch reactor model*

In order to further illuminate the influence of chemical and hydraulic input uncertainty on model predictions, we return to the batch reactor model (WS1). We demonstrate that when considering species in the bulk phase only (i.e., not including wall species), output uncertainty in a WDS can be approximated using the simple batch reactor model that only accounts for the chemical reactions, and the water age distribution at a node. We demonstrate this using WS2. We estimate output uncertainty in the batch reactor by conducting 150 MC simulations using the same set of chemical parameters used in the Chem scenario, and compare the results to the results of the Hyd1-Chem scenario within WS2.

Fig. 6 shows the monochloramine concentration as a function of water age in the batch reactor (gray lines) for the 150 simulations considering chemical uncertainty. As water age increases, so too does the variability in monochloramine concentration. This is expected since the uncertainty in monochloramine decay rate has more time to propagate.

Additionally, Fig. 6 shows the predicted monochloramine concentration and water age in WS2 for the 150 simulations considering chemical and hydraulic uncertainty. Two nodes and were selected to demonstrate the difference in monochloramine concentration for a node located near (node 258, green) and far (node 89, orange) from the source (see Fig. 3). Each marker represents the concentration and water age at each time step of each simulation. To distinguish the overlapping markers, the histograms aligned with the x-axis shows the distribution of the water age at the two nodes, demonstrating a narrower spread of the water age at node 258 compared to node 89. Similarly, the histogram aligned with the y-axis shows the distribution

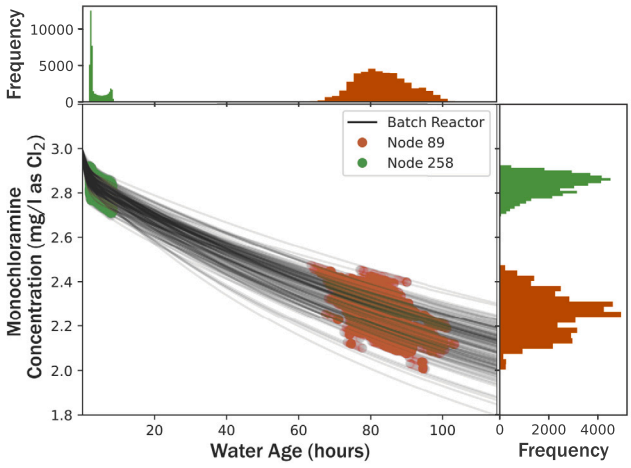

Fig. 6. Monochloramine concentrations as a function of water age in the batch reactor (gray lines), and nodes 89 (orange) and 258 (green) in WS2 at each timestep of the Hyd1-Chem scenario.

of the monochloramine concentrations at the two nodes, demonstrating similar behavior with a greater variability in concentrations as the water age increases. For Node 258, the mean water age is 3 h, and the mean monochloramine concentration is 2.83 mg/l as Cl_2 with a standard deviation of 0.04 mg/l as Cl_2, while node 89 has a mean water age of 83 h, with a mean monochloramine concentration of 2.25 mg/l as Cl_2 and a standard deviation of 0.09 mg/l as Cl_2. We observe that the monochloramine concentrations for the two nodes in the WS2 generally fall within the bounds of the concentrations simulated using the batch reactor. This result indicates that for a given water age in a WDS, monochloramine concentrations and associated uncertainty can be reasonably estimated using the simplified batch reactor model.

4. Discussion

Hydraulic uncertainty affects the water age of a parcel of water that is demanded by a user, and in turn, chemical uncertainty affects the range of potential monochloramine concentrations to be expected for a given water age. It follows that monochloramine concentration of a parcel of water demanded by a user is a function of the joint chemical and hydraulic uncertainty. The results of this study indicate the important factors to consider when determining whether hydraulic or chemical uncertainty is the main driver for the overall uncertainty in monochloramine concentrations at a given location within a WDS. The results of this work have multiple implications for water utility operations:

(1) Chemical uncertainty grows with water age because the uncertainty has more time to propagate in the chemical reaction (see Fig. 4). In addition, due to the exponential nature of monochloramine decay, a marginal increase in water age is more influential to the mean expected monochloramine concentration at lower water age than at higher water age. Therefore, accurately quantifying the water age distribution at a node is critical for characterizing monochloramine concentrations.

(2) Since the increase of uncertainty with water age is a direct cause of propagation of uncertainty of the decay reaction, as the rate of chemical decay increases (e.g., lower pH), the overall contribution of chemical uncertainty increases (see Fig. 2). Therefore, accurately characterizing chemical uncertainty in water utilities with high rates of monochloramine decay is imperative to maintaining appropriate disinfectant residual throughout-out the distribution system.

(3) Variability of monochloramine concentrations changes throughout the day, hence selecting the time of sampling can be critical for

estimating the underlying conditions in the WDS. Water quality is significantly affected by the specific path that a parcel of water takes as it travels throughout the distribution system and whether that parcel was retained in a storage tank. For example, Fig. 4d shows how the distribution of potential monochloramine concentration changes throughout the course of a day. At hour 4, there is little uncertainty in the expected monochloramine concentration, with the range of monochloramine between approximately 2.7–2.9 mg/l as Cl_2. However, at hour 11, uncertainty in monochloramine concentration is much greater, ranging between approximately 2.7–1.6 mg/l as Cl_2. Fig. 5 is used to further this analysis by showing how monochloramine concentration varies throughout the day for multiple nodes in a WDS. A water utility could use the modeling results to tailor the time of day that samples are collected at a given location at times when high uncertainty or low monochloramine concentrations is expected, in which a grab sample would provide certainty to the actual monochloramine concentration.

(4) We show that monochloramine concentration within the WDSs studied remain well above the Texas regulatory minimum value of monochloramine concentration of 0.5 mg/l as Cl_2 (Texas Administrative Code, 1977). Even with a maximum water age of approximately 200 h the minimum monochloramine concentration in WS3 was approximately 1.5 mg/l as Cl_2 (see Fig. 4d). While conditions of all WDSs vary, we demonstrate that with appropriate initial monochloramine concentration, and even when accounting for hydraulic and chemical uncertainty, monochloramine concentrations remain above regulatory standards. This method could be repeated for other chemical species and reveal areas within the distribution system which are at risk of violating the regulatory standard for that species.

(5) The comparison between WS2 and WS3 demonstrates the impact of storage and pumping on water quality within a WDS. As shown in the difference between Figs. 4, 5, and S13 in the SI, tanks contribute significantly to hydraulic uncertainty, and subsequently, to uncertainty in monochloramine levels within a WDS. Though important for maintaining hydraulic pressure regulation and storing water within the WDS, tanks contribute to increased water age within the WDS. For example, in WS3, a pump from one of the water sources was turned on/off based on the water level within the tank nearest to Node 141, exemplifying another relation between hydraulic operation and water quality within the WDS. Therefore, it is imperative to understand how the specific pumping and tank operations effect hydraulic uncertainty, and the implications for water quality in a particular WDS.

(6) Simulating and conducting uncertainty analyses of monochloramine decay in a batch reactor can provide useful insight into estimating monochloramine concentration and associated uncertainty within a WDS. By using a hydraulic model to characterize the water age at a certain location within a WDS, the influential chemical parameters can then be identified and the monochloramine concentration can be estimated using the batch reactor model without evaluating the chemical model throughout the entire distribution network (which can be computationally expensive for large networks). We note that the batch model is not a replacement for a full-scale WDS chemical model, especially if the reaction scheme includes species attached to pipe walls, or if investigating the impact of contaminant intrusion within a WDS (Hu et al., 2022; Bazargan-Lari, 2014).

4.1. Limitations and further research

There are multiple avenues for extending the proposed research. First, while the chemical reactions represented in this study are the main drivers of abiotic monochloramine decay, there are other causes of monochloramine decay. Processes, such as nitrification, and interactions with pipe walls and attached biofilms, which can contribute to the rapid decay of monochloramine, were excluded from this analysis (Wolfe et al., 1990; Wahman et al., 2016). Further studies should investigate the role of these chemical phenomena as it relates to the uncertainty in monochloramine levels within a distribution system. In addition, further research should investigate uncertainty of monochloramine decay over a wider range of water quality conditions. As previously noted, both temperature and pH are important factors which influence the rate of monochloramine decay in the unified model, and the results MC analyses would differ under conditions other than 25 °C and pH 7.75 used in this study. Finally, because the uncertainty attributed to analytical measurement of monochloramine concentration is low compared to the chemical and hydraulic mechanisms of uncertainty, this source of uncertainty was not incorporated into this study.

5. Conclusions

Coupled hydraulic and chemical models of water distribution systems can be useful tools for water utility personnel to analyze water quality within a water distribution system. However, commonly used hydraulic and water quality modeling software, such as EPANET-MSX, produce deterministic output, even though input parameters are inherently uncertain. Therefore, this work proposes a method for investigating uncertainty in water quality within a water distribution system applied to the decay of monochloramine. Specifically, this work (1) conducted a sensitivity analysis of the chemical parameters in the monochloramine decay chemical model, (2) investigated the role of chemical versus hydraulic factors in overall chemical uncertainty in two sample water distribution networks, and (3) developed a set of Python codes to implement the proposed method to be applied towards other reaction schemes, quality parameters, and water distribution networks.

The proposed chemical sensitivity analysis in a batch reactor can be used in other settings to reveal which of the chemical parameters are influential to monochloramine decay when considering the unified decay model and reactions with TOC. Thus, the parameter space can be reduced when implementing model calibration, sensitivity analysis, or other computational methods. In addition, based on the results of the MC analysis, the water age distribution at each node is the main driver in determining uncertainty related to monochloramine decay, with more uncertainty in monochloramine concentration as water age increases. Further, we show that uncertainty in monochloramine concentrations varies throughout the course of a day, and is heavily influenced by the operating conditions of storage and pumping. Hence, it is important to include system operations when evaluating water quality within WDSs. As confidence in model-based decisions for managing urban WDSs depends highly on the validity of the models, the proposed approach further emphasizes the importance of accounting for uncertainty in the context of estimating water quality in WDSs.

CRediT authorship contribution statement

Matthew Frankel: Conceptualization, Methodology, Software, Formal analysis, Writing – original draft. **Lynn E. Katz:** Writing – review & editing. **Kerry Kinney:** Writing – review & editing. **Charles J. Werth:** Writing – review & editing. **Corwin Zigler:** Writing – review & editing. **Lina Sela:** Conceptualization, Methodology, Writing – review & editing, Supervision, Funding acquisition.

Declaration of competing interest

The authors declare that they have no known competing financial interests or personal relationships that could have appeared to influence the work reported in this paper.

Data availability

The link to the codes is included in the manuscript

Acknowledgments

This work was supported by the National Science Foundation, United States under LEAP-HI Program Grant 1953206. The authors acknowledge the Texas Advanced Computing Center (TACC) at The University of Texas at Austin for providing high performance computing resources that have contributed to the research results reported in this publication. The authors also acknowledge Dr. Samuel Brodfuehrer for his input during the drafting of this manuscript.

Appendix A. Supplementary data

Supplementary material related to this article can be found online at https://doi.org/10.1016/j.jclepro.2023.137056.

References

Abhijith, G.R., Kadinski, L., Ostfeld, A., 2021. Modeling bacterial regrowth and trihalomethane formation in water distribution systems. Water 13, http://dx.doi.org/10.3390/w13040463.

Abokifa, A.A., Xing, L., Sela, L., 2020. Investigating the impacts of water conservation on water quality in distribution networks using an advection-dispersion transport model. Water 12, http://dx.doi.org/10.3390/W12041033.

Abokifa, A.A., Yang, Y.J., Lo, C.S., Biswas, P., 2016. Investigating the role of biofilms in trihalomethane formation in water distribution systems with a multicomponent model. Water Res. 104, 208–219. http://dx.doi.org/10.1016/j.watres.2016.08.006.

Agudelo-Vera, C., Avvedimento, S., Boxall, J., Creaco, E., de Kater, H., Nardo, A.D., Djukic, A., Douterelo, I., Fish, K.E., Rey, P.L.G., Jacimovic, N., Jacobs, H.E., Kapelan, Z., Solano, J.M., Pachongo, C.M., Piller, O., Quintiliani, C., Ručka, J., Tuhovčák, L., Blokker, M., 2020. Drinking water temperature around the globe: Understanding, policies, challenges and opportunities. Water (Switzerland) 12, http://dx.doi.org/10.3390/W12041049.

Alpert, S., Dussert, B.W., Mackey, E.D., Roth, D.K., Wasserstrom, L.W., 2017. 2017 Water Utility Disinfection Survey Report. American Water Works Association.

American Water Works Association, 2013. Distribution system regulations. https://www.awwa.org/portals/0/files/publications/documents/samples/20428-4e_excerpt.pdf.

Austin Water Utility, 2021. Water quality report. https://www.austintexas.gov/sites/default/files/files/Water/WaterQualityReports/AW_Water_Quality_Report_Austin_2021.pdf.

Bates, R.G., Pinching, G.D., 1950. Dissociation constant of aqueous ammonia at 0° to 50°; from e.m.f. Studies of the ammonium salt of a weak acid. J. Am. Chem. Soc..

Bazargan-Lari, M.R., 2014. An evidential reasoning approach to optimal monitoring of drinking water distribution systems for detecting deliberate contamination events. J. Clean. Prod. 78, 1–14. http://dx.doi.org/10.1016/j.jclepro.2014.04.061.

Blokker, M., Vreeburg, J., Speight, V., 2014. Residual chlorine in the extremities of the drinking water distribution system: The influence of stochastic water demands. Procedia Eng. 70, 172–180. http://dx.doi.org/10.1016/j.proeng.2014.02.020, 12th International Conference on Computing and Control for the Water Industry, CCWI2013.

Chang, N.B., Pongsanone, N.P., Ernest, A., 2012. A rule-based decision support system for sensor deployment in small drinking water networks. J. Clean. Prod. 29–30, 28–37. http://dx.doi.org/10.1016/j.jclepro.2012.02.010.

Chowdhury, S., Champagne, P., McLellan, P.J., 2009. Uncertainty characterization approaches for risk assessment of DBPs in drinking water: A review. J. Environ. Manag. 90, 1680–1691. http://dx.doi.org/10.1016/j.jenvman.2008.12.014.

Ciffroy, P., Urien, N., 2021. A probabilistic model for assessing uncertainty and sensitivity in the prediction of monochloramine loss in french river waters. Water Res. 202, http://dx.doi.org/10.1016/j.watres.2021.117383.

Dallas Water Utilities, 2021. City of dallas water quality report. https://dallascityhall.com/departments/waterutilities/DCH%20Documents/pdf/WQR2021_eng.pdf.

Di Cristo, C., Leopardi, A., de Marinis, G., 2014. Assessing measurement uncertainty on trihalomethanes prediction through kinetic models in water supply systems. J. Water Supply: Res. Technol.-Aqua 64 (5), 516–528. http://dx.doi.org/10.2166/aqua.2014.036.

Duirk, S.E., Gombert, B., Croué, J.P., Valentine, R.L., 2005. Modeling monochloramine loss in the presence of natural organic matter. Water Res. 39, 3418–3431. http://dx.doi.org/10.1016/j.watres.2005.06.003.

Frankel, M., Sela, L., 2022. MSXPY. https://github.com/mfrankel923/MSXPY.

Frankel, M., Xing, L., Chewning, C., Sela, L., 2021. Water-energy benchmarking and predictive modeling in multi-family residential and non-residential buildings. Appl. Energy 281, http://dx.doi.org/10.1016/j.apenergy.2020.116074.

Gibson, J., Karney, B., Guo, Y., 2020. Effects of demand, mixing fraction, and rate coefficient uncertainty on water quality models. J. Water Resour. Plan. Manag. http://dx.doi.org/10.1061/(ASCE)WR.1943.

Granstrom, M., 1955. The Disproportionation of Monochloramine (Ph.D. thesis). Harvard University.

Hand, V.C., Margerum, D.W., 1983. Kinetics and mechanisms of the decomposition of dichloramine in aqueous solution. Inorg. Chem. 22, 47907.

Hart, D., Rodriguez, J.S., Burkhardt, J., Borchers, B., Laird, C., Murray, R., Klise, K., Haxton, T., 2019. Quantifying hydraulic and water quality uncertainty to inform sampling of drinking water distribution systems. J. Water Resour. Plan. Manag. 145, 04018084. http://dx.doi.org/10.1061/(asce)wr.1943-5452.0001005.

Hatam, F., Ebacher, G., Prévost, M., 2021. Stringency of water conservation determines drinking water quality trade-offs: Lessons learned from a full-scale water distribution system. Water (Switzerland) 13, http://dx.doi.org/10.3390/w13182579.

Herman, J.D., Kollat, J.B., Reed, P.M., Wagener, T., 2013. Technical note: Method of morris effectively reduces the computational demands of global sensitivity analysis for distributed watershed models. Hydrol. Earth Syst. Sci. 17, 2893–2903. http://dx.doi.org/10.5194/hess-17-2893-2013.

Herman, J., Usher, W., 2017. Salib: An open-source python library for sensitivity analysis. J. Open Source Softw. 2 (9), http://dx.doi.org/10.21105/joss.00097.

Houston Public Works, 2021. Houston water quality report 2021. https://www.houstonpublicworks.org/sites/g/files/nwywnm456/files/doc/003-water-quality-report-2021.pdf.

Hu, Z., Chen, W., Tan, D., Ye, S., Shen, D., 2022. Multi-objective model for optimal sensor placement in water distribution systems considering contamination probability variation-based contaminant impact. J. Clean. Prod. 372, http://dx.doi.org/10.1016/j.jclepro.2022.133445.

Iwanaga, T., Usher, W., Herman, J., 2022. Toward salib 2.0: Advancing the accessibility and interpretability of global sensitivity analyses. Soc.-Environ. Syst. Model. 4, 18155. http://dx.doi.org/10.18174/sesmo.18155.

Jafvert, C.T., 1985. A Unified Chlorine-Ammonia Speciation and Fate Model (Ph.D. thesis). University of Iowa.

Jafvert, C.T., Valentine, R.L., 1987. Dichloramine decomposition in the presence of excess ammonia. Water Resour. 21, 967–973.

Jafvert, C.T., Valentine, R.L., 1992. Reaction scheme for the chlorination of ammoniacal water. Environ. Sci. Technol. 26, 577–585.

Khiari, D., 2019. The Role and Behavior of Chloramines in Drinking Water. The Water Research Foundation.

Leao, S.F., 1981. Kinetics of Combined Chlorine: Reactions of Substitution and Redox (Ph.D. thesis). University of California, Berkeley.

Li, R.A., McDonald, J.A., Sathasivan, A., Khan, S.J., 2019. Disinfectant residual stability leading to disinfectant decay and by-product formation in drinking water distribution systems: A systematic review. Water Res. 153, 335–348. http://dx.doi.org/10.1016/j.watres.2019.01.020.

Lytle, D.A., Liggett, J., 2016. Impact of water quality on chlorine demand of corroding copper. Water Res. 92, 11–21. http://dx.doi.org/10.1016/j.watres.2016.01.032.

Margerum, D.W., Gray, E.T., Huffman, R.P., 1978. Chlorination and the formation of N-chloro compounds in water treatment. Am. Chem. Soc..

Masters, S., Parks, J., Atassi, A., Edwards, M.A., 2016. Inherent variability in lead and copper collected during standardized sampling. Environ. Monit. Assess. 188, 1–15. http://dx.doi.org/10.1007/s10661-016-5182-x.

Mckay, M.D., Beckman, R.J., Conover, W.J., 1979. A comparison of three methods for selecting values of input variables in the analysis of output from a computer code. Technometrics 21, 239–245.

Morris, C., 1966. The acid ionization constant of HOCI from 5 to 35°. J. Phys. Chem. 70, 3798–3805.

Morris, J.C., Isaac, R.A., 1983. A critical review of kinetic and thermodynamic constants for the aqueous chlorine-ammonia system. Water Chlorination Environ. Impact Health Eff. - Chem. Water Treat. 4, 49–62.

Ormsbee, L., Hoagland, S., Hernandez, E., Hall, A., Ostfeld, A., 2022. Hydraulic model database for applied water distribution systems research. J. Water Resour. Plan. Manag. 148, http://dx.doi.org/10.1061/(asce)wr.1943-5452.0001559.

Ozekin, K., Valentine, R.L., Vikesland, P.J., 1996. Modeling the decomposition of disinfecting residuals of chloramine. Am. Chem. Soc. 115–125.

Pankaj, B.S., Jaykrishnan, G., Ostfeld, A., 2022. Optimizing water quality treatment levels for water distribution systems under mixing uncertainty at junctions. J. Water Resour. Plan. Manag. 148, http://dx.doi.org/10.1061/(ASCE)WR.1943-5452.0001544.

Pannier, M.L., Schalbart, P., Peuportier, B., 2018. Comprehensive assessment of sensitivity analysis methods for the identification of influential factors in building life cycle assessment. J. Clean. Prod. 199, 466–480. http://dx.doi.org/10.1016/j.jclepro.2018.07.070.

Pasha, M.F., Lansey, K., 2010. Effect of parameter uncertainty on water quality predictions in distribution systems- case study. J. Hydroinform. 12, 1–21. http://dx.doi.org/10.2166/hydro.2010.053.

Peter, K.O., Vikesland, J.Y., Valentine, R.L., 2001. Monochloramine dacay in model and distribution system waters. Water Resour. 35, 1766–1776.

Pfaller, S., King, D., Mistry, J.H., Alexander, M., Abulikemu, G., Pressman, J.G., Wahman, D.G., Donohue, M.J., 2021. Chloramine concentrations within distribution systems and their effect on heterotrophic bacteria, mycobacterial species, and disinfection byproducts. Water Res. 205, http://dx.doi.org/10.1016/j.watres.2021.117689.

Ricca, H., Aravinthan, V., Mahinthakumar, G., 2019. Modeling chloramine decay in full-scale drinking water supply systems. Water Environ. Res. 91, 441–454. http://dx.doi.org/10.1002/wer.1046.

Rodriguez, J.S., Bynum, M., Laird, C., Hart, D.B., Klise, K.A., Burkhardt, J., Haxton, T., 2021. Optimal sampling locations to reduce uncertainty in contamination extent in water distribution systems. J. Infrastruct. Syst. 27, 04021026. http://dx.doi.org/10.1061/(asce)is.1943-555x.0000628.

Rossman, L., Woo, H., Tryby, M., Shang, F., Janke, R., Haxton, T., 2020. EPANET 2.2 User Manual. Tech. Rep. EPA/600/R-20/133, U.S. Environmental Protection Agency, Washington, D.C..

Roy, R., Sathasivan, A., Kastl, G., 2020. Simplified chemical chloramine decay model for water distribution systems. Sci. Total Environ. 741, http://dx.doi.org/10.1016/j.scitotenv.2020.140410.

Ruano, M.V., Ribes, J., Seco, A., Ferrer, J., 2012. An improved sampling strategy based on trajectory design for application of the morris method to systems with many input factors. Environ. Model. Softw. 37, 103–109. http://dx.doi.org/10.1016/j.envsoft.2012.03.008.

Saltelli, A., Tarantola, S., Campolongo, F., Ratto, M., 2004. Global Sensitivity Analysis. The Primer. John Wiley & Sons, Ltd.

Shang, F., Uber, J.G., Rossman, L.A., 2008. Modeling reaction and transport of multiple species in water distribution systems. Environ. Sci. Technol. 42, 808–814. http://dx.doi.org/10.1021/es072011z.

Silva, A.S., Ghisi, E., 2020. Estimating the sensitivity of design variables in the thermal and energy performance of buildings through a systematic procedure. J. Clean. Prod. 244, http://dx.doi.org/10.1016/j.jclepro.2019.118753.

Smith, R.C., 2013. Uncertainty Quantification: Theory, Implementation, and Applications. Society for Industrial and Applied Mathematics, Philadelphia, PA, USA.

Snoeyink, V., Jenkins, D., 1980. Water Chemistry. John Wiley & Sons, New York, N.Y..

Spearing, L.A., Thelemaque, N., Kaminsky, J.A., Katz, L.E., Kinney, K.A., Kirisits, M.J., Sela, L., Faust, K.M., 2021. Implications of social distancing policies on drinking water infrastructure: An overview of the challenges to and responses of U.S. utilities during the COVID-19 pandemic. ACS EST Water 1, 888–899. http://dx.doi.org/10.1021/acsestwater.0c00229.

TACC - Texas Advanced Computing Center, 2020. Stampede 2 user guide. https://portal.tacc.utexas.edu/user-guides/stampede2.

Texas Administrative Code, 1977. Rule 290.110. https://texreg.sos.state.tx.us/public/readtac$ext.TacPage?sl=R&app=9&p_dir=&p_rloc=&p_tloc=&p_ploc=&pg=1&p_tac=&ti=30&pt=1&ch=290&rl=110.

Tiemann, M., 2017. Safe Drinking Water Act (SDWA): A Summary of the Act and its Major Requirements. Congressional Research Service, Washington, DC.

Tong, Y.L., 2012. The Multivariate Normal Distribution. Springer Science & Business Media.

U.S. Environmental Protection Agency, 2002. Effects of water age on distribution system water quality. https://www.epa.gov/sites/default/files/2015-09/documents/2007_05_18_disinfection_tcr_whitepaper_tcr_waterdistribution.pdf.

Wahman, D.G., 2018. Web-based applications to simulate drinking water inorganic chloramine chemistry. Am. Water Works Assoc. 110, E43–E61.

Wahman, D.G., Maestre, J.R., Speitel, G.E., 2016. Monochloramine cometabolism by nitrifying biofilm relevant to drinking water. J. - Am. Water Works Assoc. 108, E362–E373. http://dx.doi.org/10.5942/jawwa.2016.108.0092.

Wahman, D.G., Speitel, G.E., 2012. Relative importance of nitrite oxidation by hypochlorous acid under chloramination conditions. Environ. Sci. Technol. 46, 6056–6064. http://dx.doi.org/10.1021/es300934x.

Wolfe, R.L., Lieu, N.I., Izaguirre, G., Means, E.G., 1990. Ammonia-oxidizing bacteria in a chloraminated distribution system: Seasonal occurrence, distribution, and disinfection resistance. Appl. Environ. Microbiol. 56, 451–462. http://dx.doi.org/10.1128/aem.56.2.451-462.1990.

Yang, J., 2011. Convergence and uncertainty analyses in Monte-Carlo based sensitivity analysis. Environ. Model. Softw. 26, 444–457. http://dx.doi.org/10.1016/j.envsoft.2010.10.007.

Zhang, D., Bond, T., Pan, Y., Li, M., Luo, J., Xiao, R., Chu, W., 2022. Identification, occurrence, and cytotoxicity of haloanilines: A new class of aromatic nitrogenous disinfection byproducts in chloraminated and chlorinated drinking water. Environ. Sci. Technol. 56, 4132–4141. http://dx.doi.org/10.1021/acs.est.1c07375.

Zhuang, J., Sela, L., 2020. Impact of emerging water savings scenarios on performance of urban water networks. J. Water Resour. Plan. Manag. 146, 04019063. http://dx.doi.org/10.1061/(asce)wr.1943-5452.0001139.

Supporting Information for

Framework for Assessing Uncertainty of Water Quality in Distribution Networks Applied to Monochloramine Decay

Matthew Frankel[1], Lynn Katz[1], Kerry Kinney[1], Charles Werth[1], Corwin Zigler[2], Lina Sela[1]

[1]Department of Civil, Architectural and Environmental Engineering, The University of Texas at Austin

[2]Departments of Statistics and Data Science, the University of Texas at Austin

Contents of this file

Introduction

Figures and tables included in the main text were chosen to convey findings, and also to maintain brevity. The additional information in this file reports additional findings from our work that are not essential for understanding the experimental results, but bolster our findings and support claims made in the main text. Figures include a depiction of the level of influence of chemical parameters at differing levels of pH, classification of users within each water system, and results of a MC simulation for WS2.

S1. Morris Method – Illustrative Example

An example of the implementation of the Morris method is presented for the arbitrary function f(x), with three input parameters: x_1, x_2, and x_3. Suppose that the bounds $[L_i, U_i]$ for each parameter are [0,12], [400,520], and [22,25], respectively, and the values of p, δ and r are 4, 2/3, and 3, respectively. Table S1 shows the three trajectories, input parameters to be used in each model evaluation, and value of f(x) for each set of input parameters. Trajectory 1 starts with a random sample x = (0,440,22). Then, in the next step, only x_2 is modified by $\frac{2}{3}(520 - 400) = 80$, and the function f(x) is evaluated. In the next step of trajectory 1, x_1 is perturbed by $\frac{2}{3}(12 - 0) = 8$ and the rest of the parameters are kept constant. Finally, x_3 is perturbed by $\frac{2}{3}(25 - 22) = 2$ and f(x) is evaluated again. This completes one trajectory. For each parameter x_i, one elementary effect per trajectory is calculated. The elementary effects of parameter x_1 are calculated based on Eq. 1 using model evaluations f(x) (see Table S1). For example, the first elementary effect of parameter x_1, using function evaluations 2 and 3, is calculated as $d_{11} = \frac{780-716}{\frac{2}{3}} = 960$. Similarly, the second and third elementary effects can be calculated based on model evaluations 6 and 7, and 10 and 11, respectively, with $d_{21} = 96$ and $d_{31} = 192$. Then, μ_1^* is computed as the absolute mean of all elementary effects for parameter 1, i.e., $128 = \frac{96+96+192}{3}$. Similarly, $\mu_2^* = 432$ and $\mu_3^* = 198$, indicating the influence of each parameter relative to the other parameters. In this particular case, the function f(x) is most sensitive to the value of x_2, least sensitive to x_1, and slightly more sensitive to x_3 than x_1. The values of σ are 55.4, 31.2, and 31.2 for parameters x_1, x_2, and x_3, respectively, which indicate that x_1 has the highest level of interaction with the other parameters. Values of σ are equal for x_2 and x_3, indicating that there is equal level of interaction of x_2 and x_3 with other parameters.

Table S1: Function evaluations to demonstrate the Morris method for an arbitrary function f(x), based on three input parameters: x_1, x_2, and x_3}

Trajectory	Model Evaluation	x_1	x_2	x_3	f(x)
1	1	0	440	22	452
	2	0	520	22	716
	3	8	520	22	780
	4	8	520	24	936
2	5	8	400	23	444
	6	8	400	25	564
	7	0	400	25	500
	8	0	480	25	800
3	9	12	400	23	524
	10	12	400	25	644
	11	4	400	25	516
	12	4	480	25	816

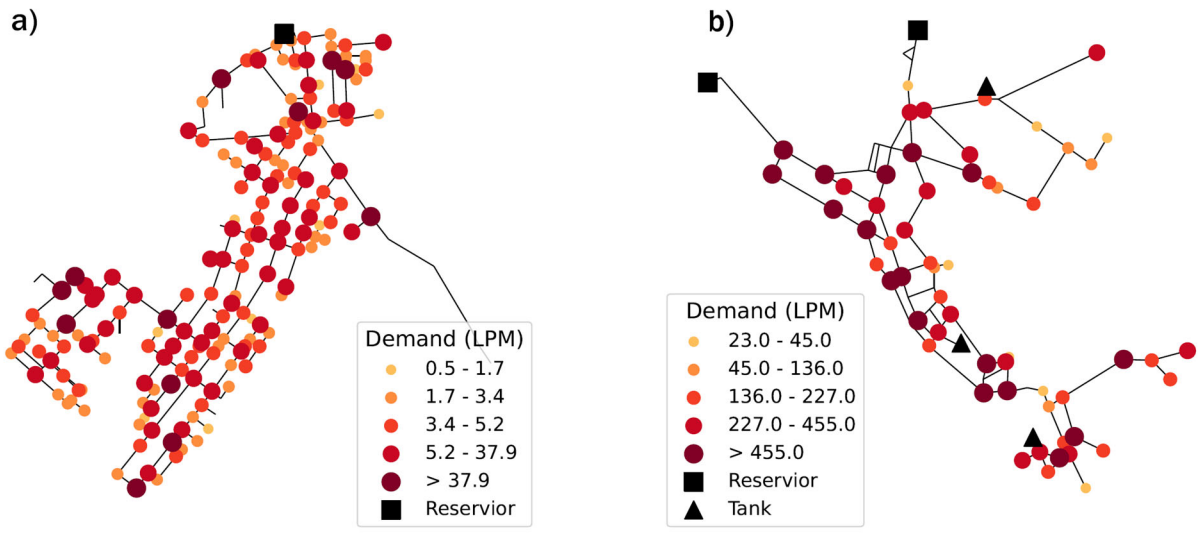

Figure S1: Layout, locations of reservoirs and tanks, and magnitude of demands at each node for: (a) WS2 and (b) and WS3.

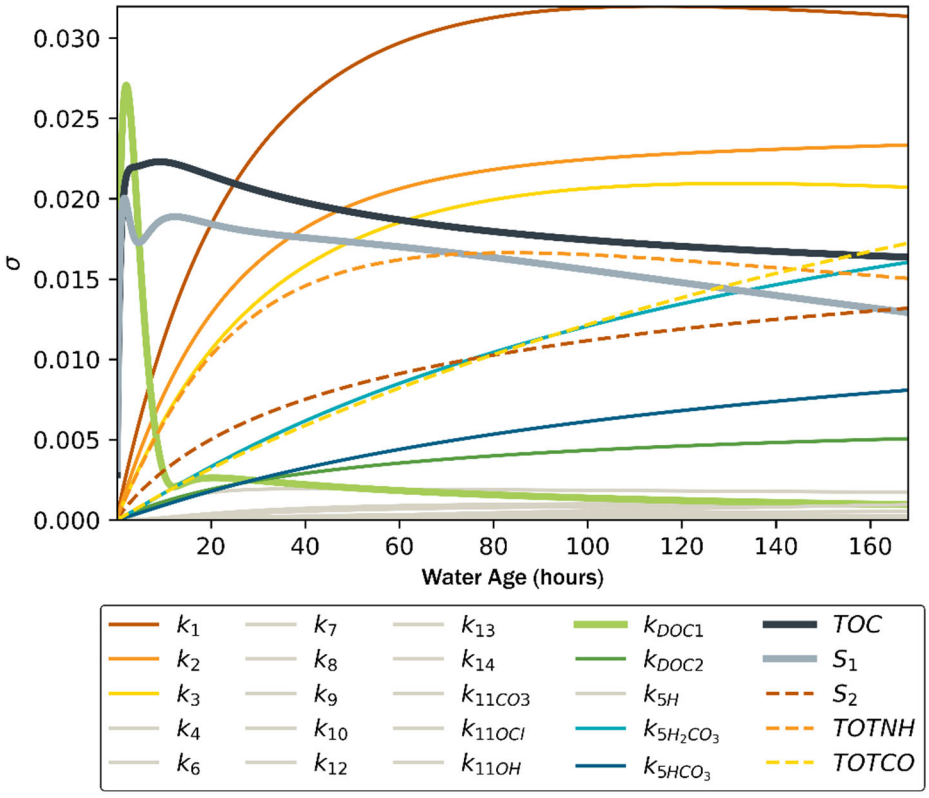

Figure S2: Level of interaction between each parameter and all other parameters, indicated by sigma, for all parameters at pH 7.75

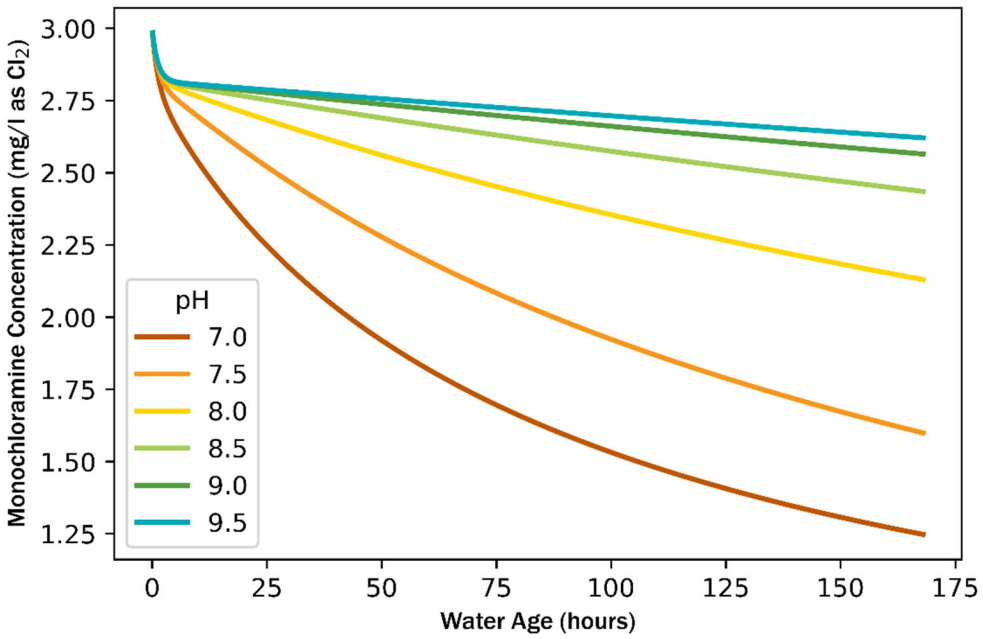

Figure S3: Monochloramine decay at varying levels of pH, with all other parameters values constant, demonstrating the effect of pH on monochloramine decay rate

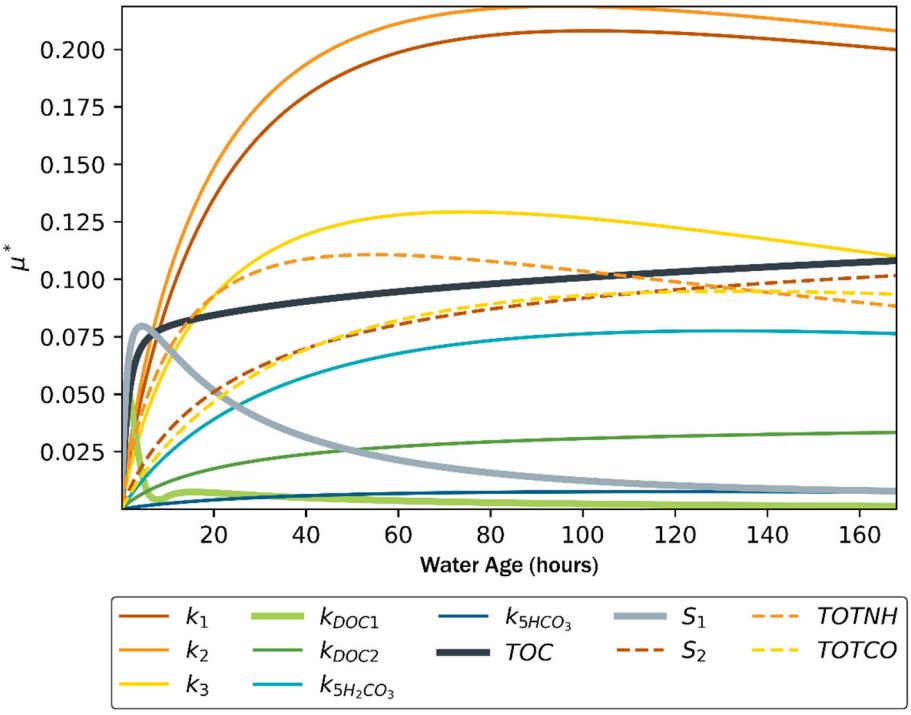

Figure S4: Results of Method of Morris applied to the Batch model at pH 7, with parameter-specific uncertainty ranges

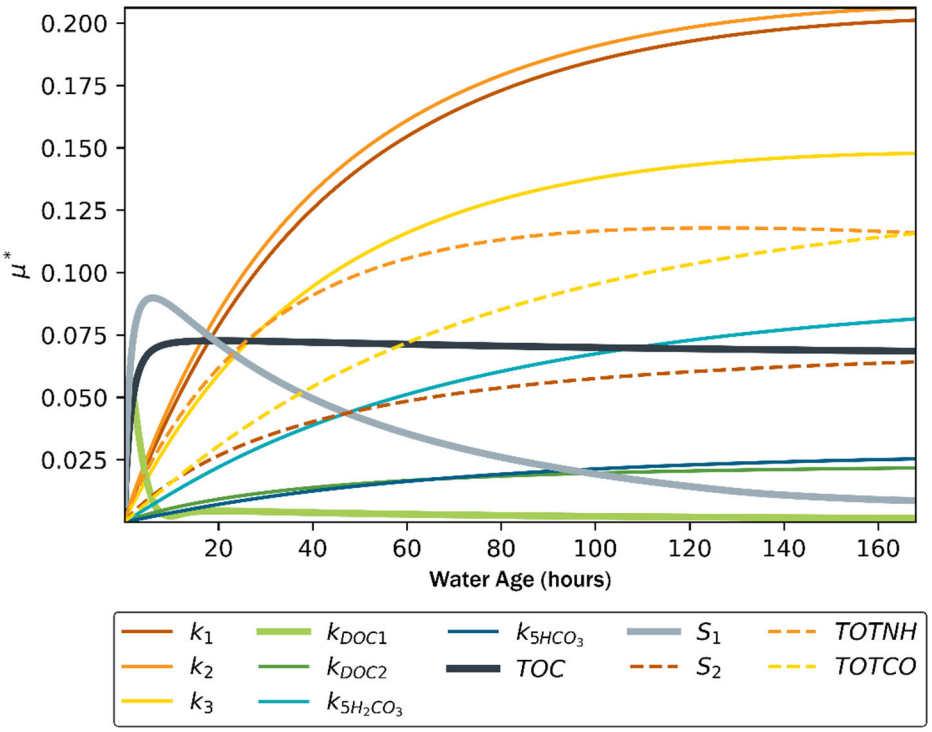

Figure S5: Results of Method of Morris applied to the Batch model at pH 7.5, with parameter-specific uncertainty ranges

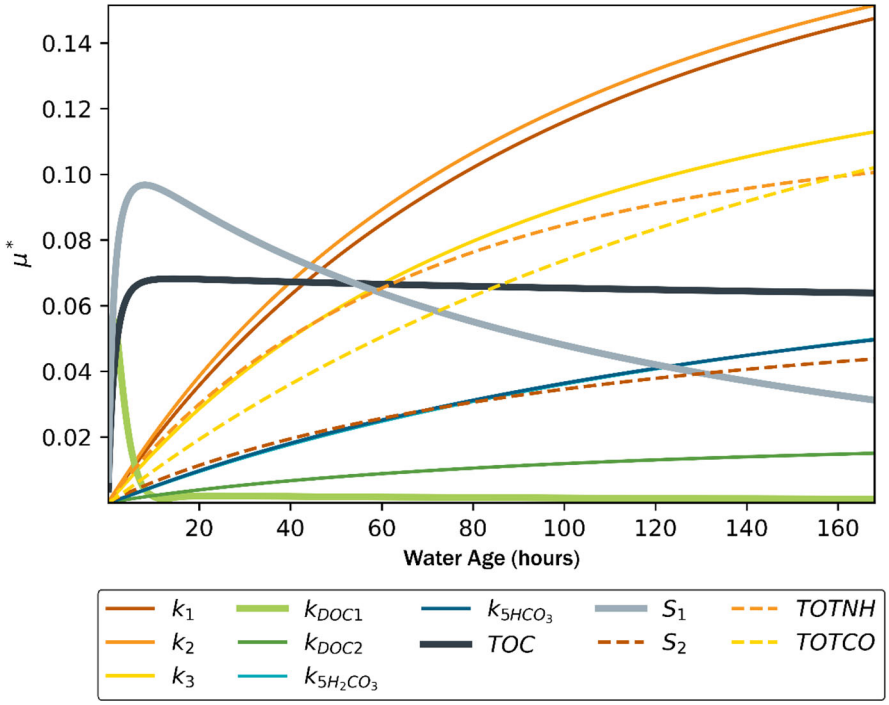

Figure S6: Results of Method of Morris applied to the Batch model at pH 8, with parameter-specific uncertainty ranges

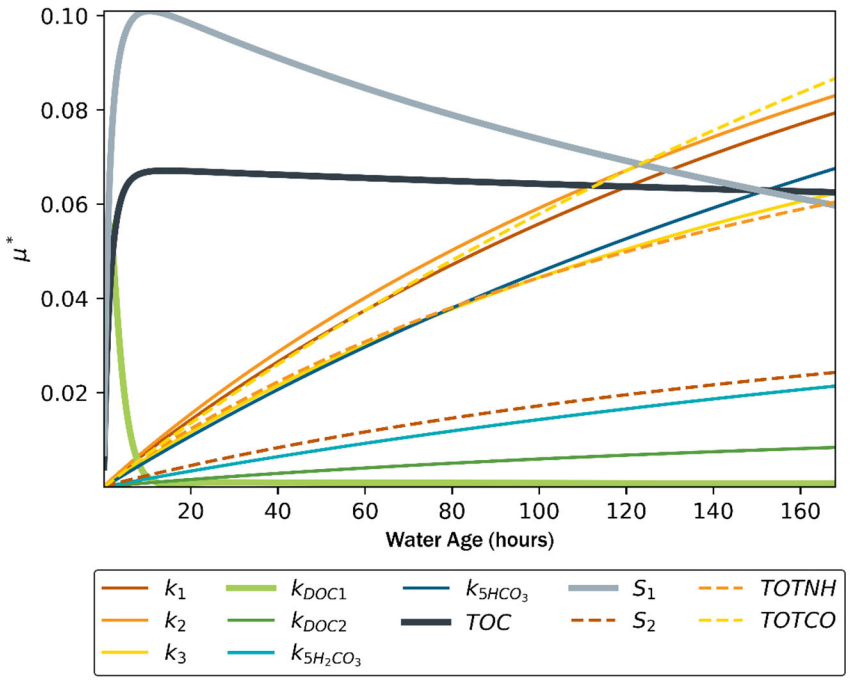

Figure S7: Results of Method of Morris applied to the Batch model at pH 8.5, with parameter-specific uncertainty ranges

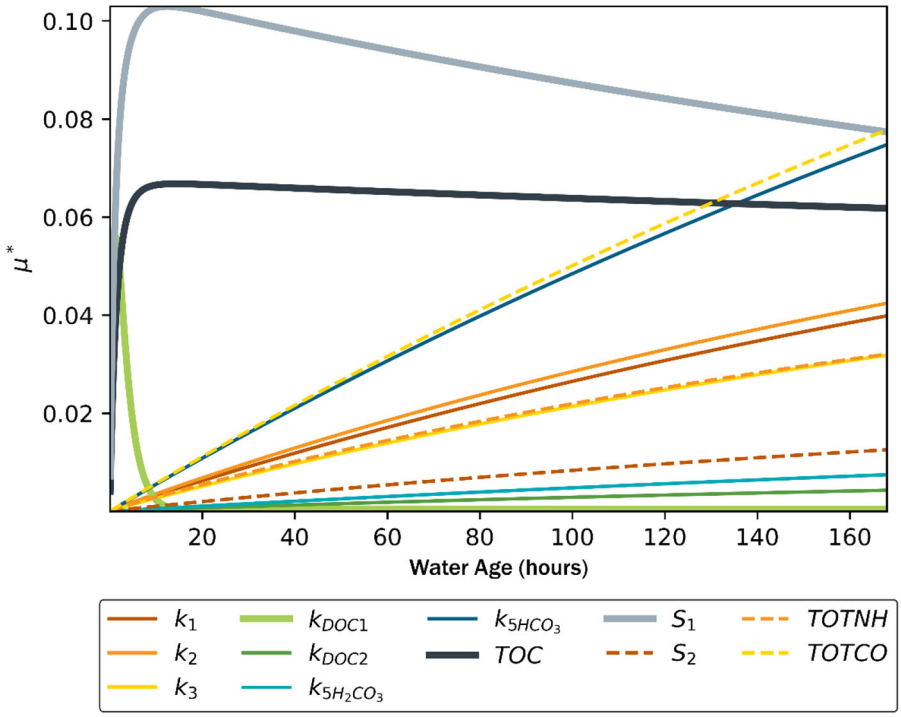

Figure S8: Results of Method of Morris applied to the Batch model at pH 9, with parameter-specific uncertainty ranges

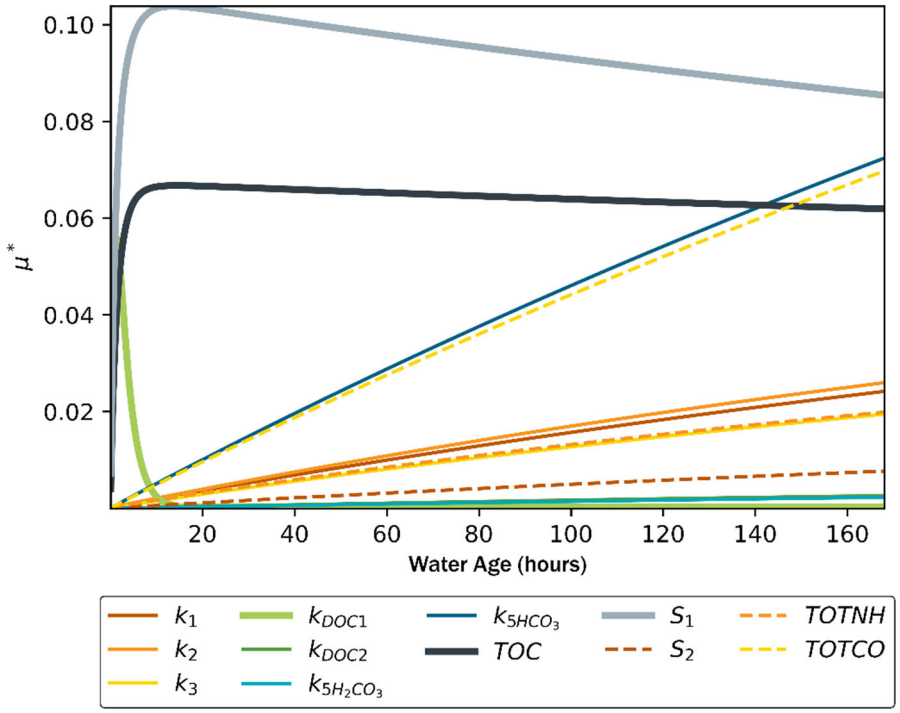

Figure S9: Results of Method of Morris applied to the Batch model at pH 9.5, with parameter-specific uncertainty ranges

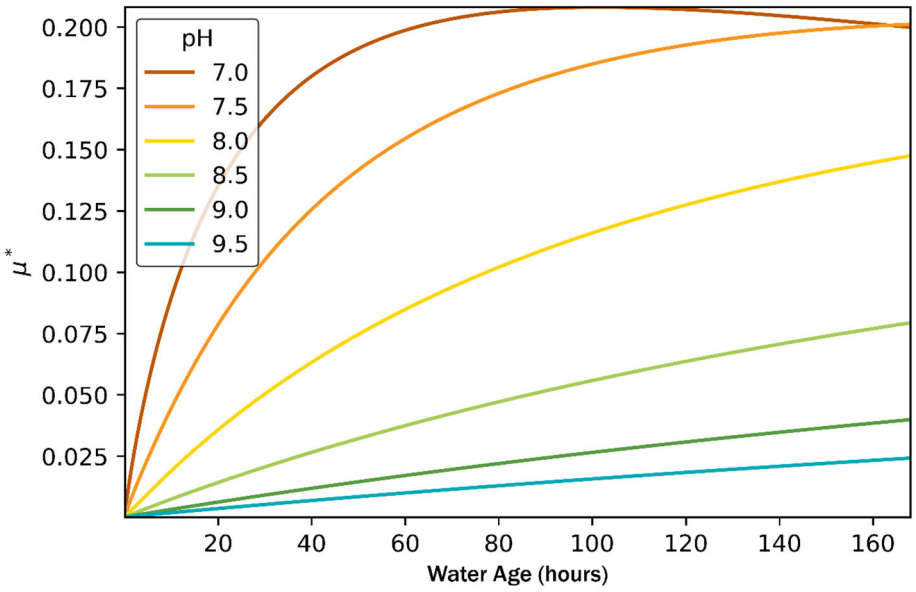

Figure S10: Influence of parameter k_1 on monochloramine decay at levels of pH between 7 and 9.5

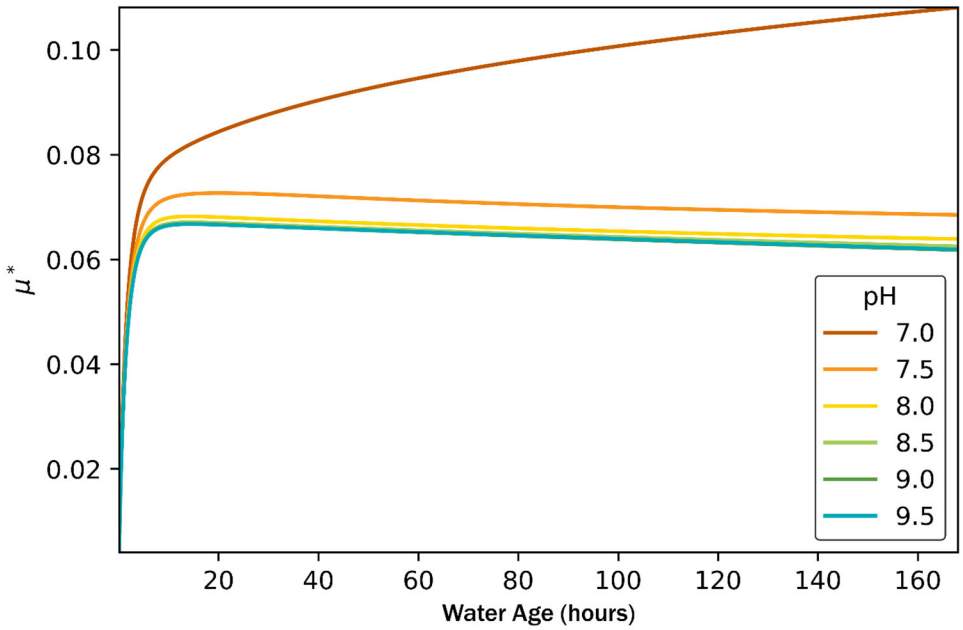

Figure S11: Influence of parameter TOC on monochloramine decay at levels of pH between 7 and 9.5

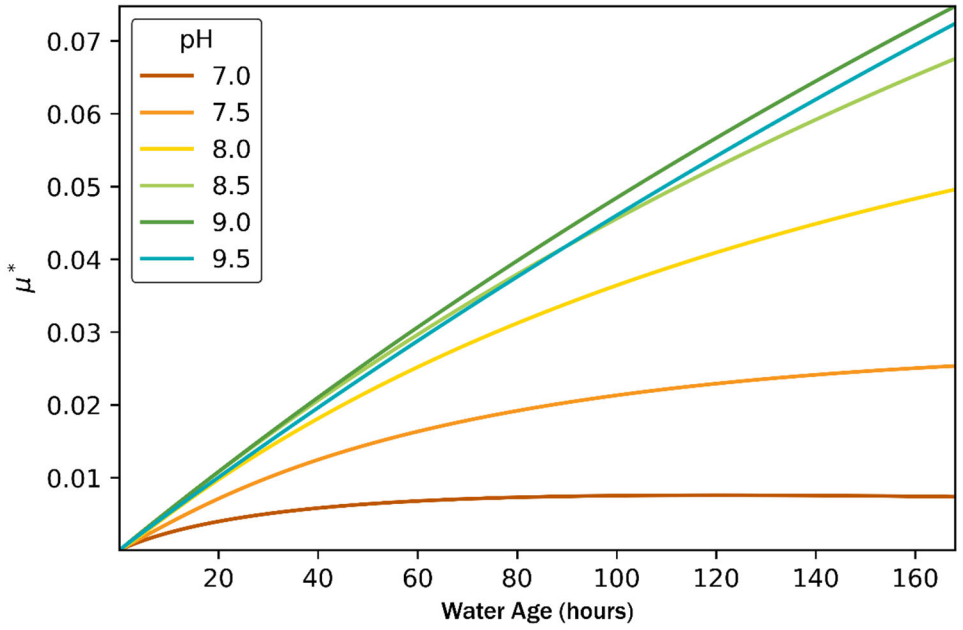

Figure S12: Influence of parameter $k_{5H_2CO_3}$ on monochloramine decay at levels of pH between 7 and 9.5

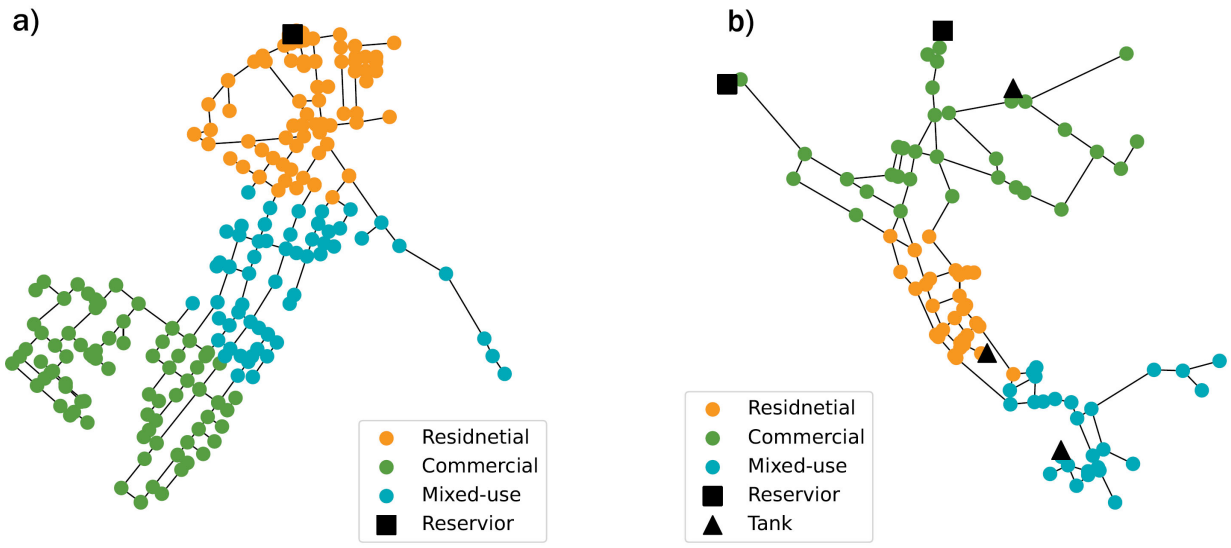

Figure S13: Assignment of user groups to each node in (a) WS2 and (b) WS3

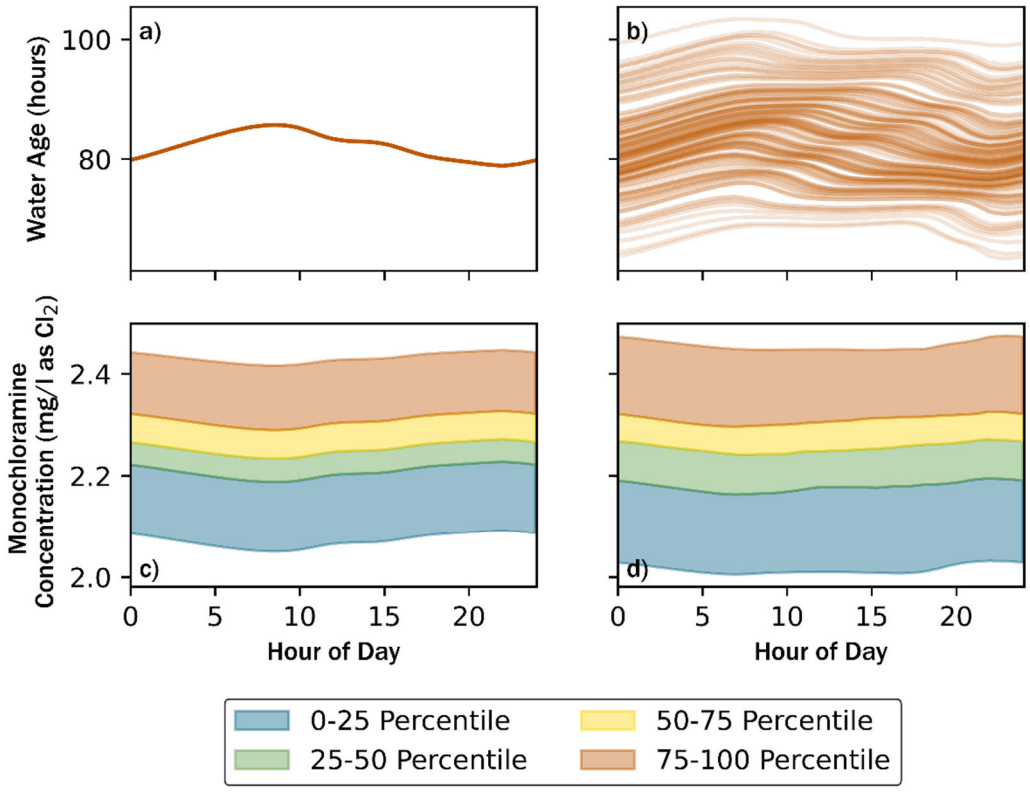

Figure S14: Results at node 89 in WS2: (a) predicted water age with chemical uncertainty, (b) predicted water age with chemical and hydraulic uncertainty, (c) predicted monochloramine concentrations with chemical uncertainty, (d) predicted monochloramine concentrations with chemical and hydraulic uncertainty.

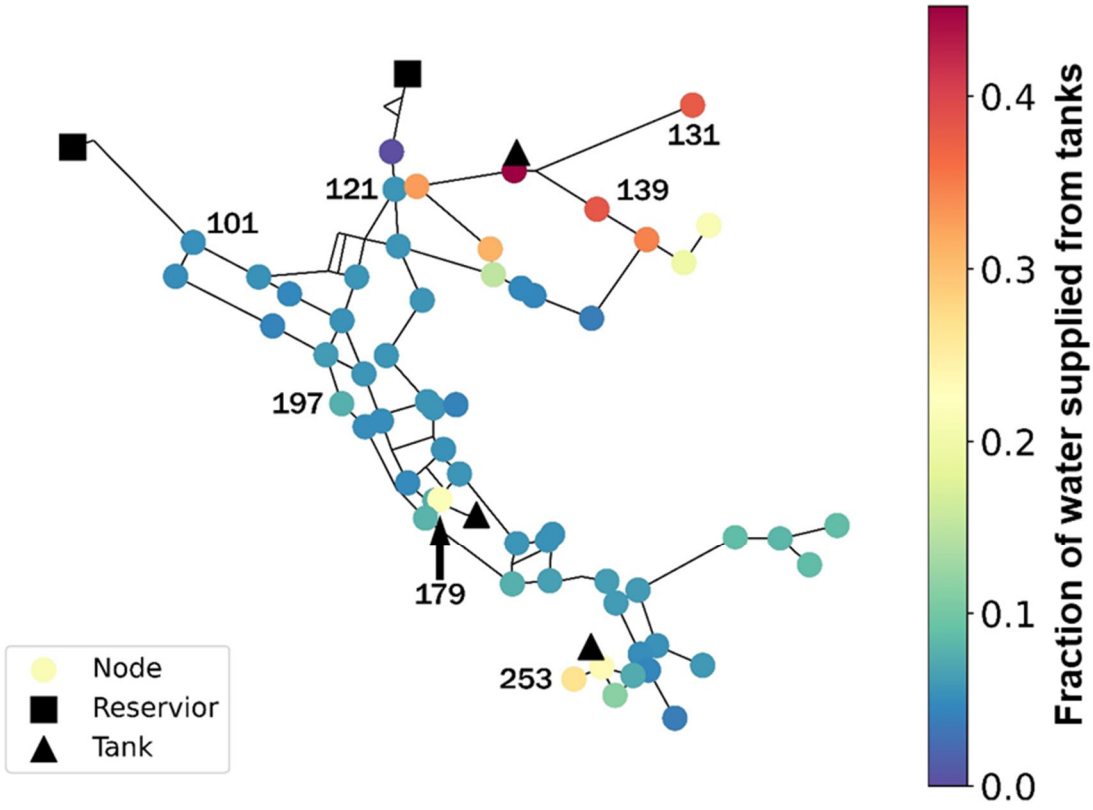

Figure S15: Fraction of water supplied from tanks to each node in WS3 over the course of a 24-hour period. A value of 0.4 indicates that on average, 40% of the water demanded at that node was supplied from a storage tank and 60% directly from the source. Node labels correspond to the nodes shown in Figure 5.